UNCLASSIFIED

AD 296 366

*Reproduced
by the*

ARMED SERVICES TECHNICAL INFORMATION AGENCY
ARLINGTON HALL STATION
ARLINGTON 12, VIRGINIA

THE ORIGINAL PRINTING OF THIS DOCUMENT

CONTAINED COLOR WHICH ASTIA CAN ONLY

REPRODUCE IN BLACK AND WHITE

UNCLASSIFIED

CR-61-419-1F

UNCLASSIFIED

BROADBAND S-BAND REACTANCE AMPLIFIER

Report Number Six

FINAL PROGRESS REPORT

1 July 1960 - 7 March 1962

Signal Corps Contract DA 36-039-sc-85058

DA Project No. 3A99-21-001-01

1 September 1962

STIA

SEP 13 1963

TISIA
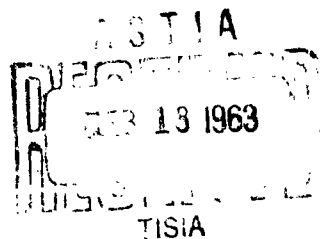
Prepared for: U. S. Army Signal Research & Development
Laboratory
Fort Monmouth, New Jersey

Prepared by: Surface Communications Systems Laboratory
Defense Electronic Products
Radio Corporation of America
75 Varick Street
New York 13, New York

UNCLASSIFIED

DEFENSE ELECTRONIC PRODUCTS
SURFACE COMMUNICATIONS DIVISION
CAMDEN, NEW JERSEY

SURFACE

COMMUNICATIONS

NO OTS

Report Number Six

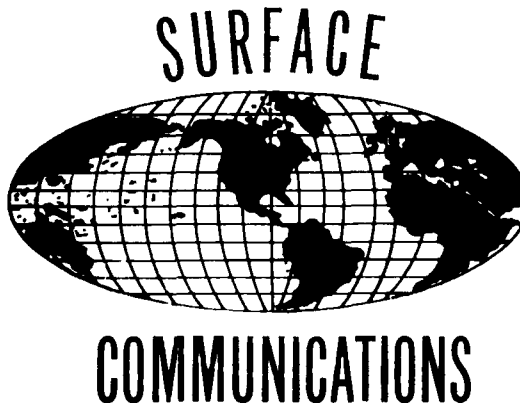BROADBAND S-BAND REACTANCE AMPLIFIER

Covering the period 1 July 1960 - 7 March 1962

FINAL PROGRESS REPORT

1 September 1962

Signal Corps Contract DA 36-039-sc-85058

DA Project No. 3A99-21-001-01

RCA Report No. CR-61-419-1F

Signal Corps Specification Number SCL-7556 Dated 7 March 1960

Object: To experimentally and theoretically investigate

the feasibility of a broadband, low-noise, S-band

reactance amplifier

Report Written by: B. Bossard
                      R. M. Kurzrok
                      E. Markard
                      B. Perlman
                      R. Pettai

Prepared by: Surface Communications Systems Laboratory
               Defense Electronic Products
               Radio Corporation of America
               75 Varick Street
               New York 13, New York

TABLE OF CONTENTS

LIST OF FIGURES

LIST OF FIGURES (Continued)

SECTION 1: PURPOSE

The purpose of this investigation is to develop a low-noise, broadband, S-band reactance amplifier. Three approaches have been employed: filter-type parametric upconverters using a single diode; filter-type circulator-coupled parametric amplifiers using a single diode; and, finally, a circulator-coupled paramp using two diodes in a balanced structure. The balanced scheme was initially described and developed by Airborne Instruments Laboratory.

This program is an extension of the state of the art in which design goals entail 13-db minimum gain, 2 kmc to 4 kmc minimum bandwidth and an amplifier noise figure less than 2 db. An engineering model is desired having performance substantially in accordance with these design goals. (Reference: Signal Corps Specification SCL-7556 dated 7 March 1960.)

SECTION 2: ABSTRACT

A substantial amount of small signal and large signal theoretical work has been carried out for the broadbanding of microwave parametric amplifiers. Theoretical results have yielded single-diode voltage-gain-bandwidth products of 3500 mc at "S" band. It is concluded that the simulation of broadband paramps by appropriate lumped-circuit elements is handicapped at microwave frequencies where inductances and capacitances must be simulated by distributed elements. Moreover, the sections of transmission line coupling the individual network elements to the varactor diode have frequency sensitivities of their own which must be considered in transforming a lumped-element design into a distributed microwave equivalent, especially when broad (20 - 50%) bandwidths are involved.

Broadband paramps can be constructed, however, by making maximum use of the varactor parasitic elements in a filter structure at the plane of the diode. (No coupling lengths of line are required.) Techniques have been developed which allow the varactor diode to exhibit two simultaneous resonant frequencies (at signal and idler) depending upon the geometry of the holding structure. Novel experimental techniques were conceived on the subject program that permit rapid determination of the diode resonances and matching conditions. The gain bandwidth product of a given diode can be evaluated by passive measurements. Preliminary experimental efforts on parametric amplifiers employing the above principles have yielded single-diode voltage-gain-bandwidth products of 3300 mc at "S" band.

SECTION 3: PUBLICATIONS, LECTURES, REPORTS, AND CONFERENCES

A fifth quarterly report on this program has already been issued. On 2 February 1962, Mr. B. Bossard delivered at the AIEE Winter Meeting, an invited technical paper entitled "Parametric Amplifiers", which was jointly authored with Mr. R. Pettai. A paper by Messrs. Bossard and Pettai, entitled "Broadband Parametric Amplifiers by Simple Experimental Techniques", has been published in the March 1962 Proceedings of the IRE. A paper by Messrs. Bossard and Pettai, entitled "Broadband Parametric Amplifiers" has been presented at the 1962 PGMTT Symposium at Boulder, Colorado. A paper by Messrs. Bossard and Perlman, entitled "Electronically Tunable Parametric Amplifiers", is to be published in the IRE Proceedings. All of these papers are based upon significant work done on this program.

On 19 December 1961, Mr. S. J. Mehlman, Mr. R. M. Kurzrok, Mr. B. Bossard and Mr. R. Pettai, all of RCA, visited Mr. W. Matthei and Mr. F. Senko of USASRDL. Technical progress on the program was briefly discussed and a broadband, circulator-coupled parametric amplifier was demonstrated. This unit displayed performance substantially in accord with the results tabulated in this report.

On 12 February 1962, Mr. F. Senko of USASRDL and Mr. J. Kliphuis of Airborne Instruments Laboratory visited RCA. In an informal conference attended by B. Bossard and R. Pettai of RCA, Mr. Kliphuis discussed certain characteristics of the AIL balanced parametric amplifier; paramp techniques developed at RCA on the subject program were also discussed. The material exchange of technical information resulted in a better understanding by all concerned, with respect to the subtleties of broadband microwave parametric

amplifiers.

A broadband parametric amplifier with a gain of 10 db throughout a bandwidth of 850 mc was demonstrated in the AN/TUR-1 Receiver at Sandy Hook, New Jersey to Signal Corps Personnel. A 9-db improvement in minimum detectable signal was apparent throughout the paramp bandwidth. The amplifier exhibited excellent stability and linearity and did not produce any noticeable cross or third-order intermodulation characteristics for jamming signals as large as 15 dbm.

SECTION 4: FACTUAL DATA

During this project a number of possible approaches were investigated in order to find the type of structure and the mode of operation which would yield the widest bandwidth at a reasonable gain. In the following chapters all the approaches studied are described in some detail, with most of the attention devoted to the final structure and its theory.

CHAPTER I. GENERAL THEORY AND NETWORK SYNTHESIS APPROACH TO BROADBAND PARAMETRIC AMPLIFICATION

The first phase of the program was devoted to the theoretical investigation of the varactor parameters and their influence on broadband parametric amplification. The following varactor equivalent circuit yielded the Y matrix as shown. (See Appendix I for derivation.)
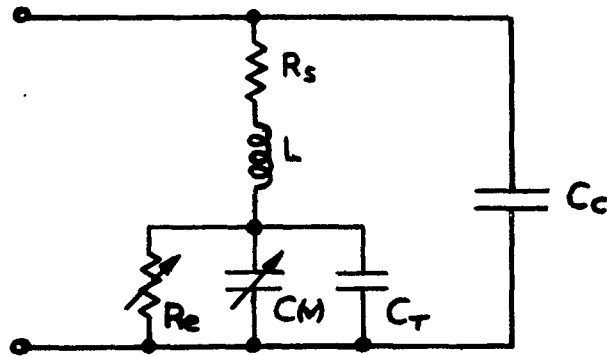
Figure 4-1. Equivalent Circuit of a Varactor Diode

$$\|Y\| = \frac{1}{D} \left\| \begin{array}{cc} j\omega_1 C_T\left[1-K^2(\beta_2^2+j\epsilon_2)\right] & j\omega_1\left(\frac{\Delta C}{2}\right) \\ -j\omega_2\left(\frac{\Delta C}{2}\right) & -j\omega_2 C_T\left[1-K^2(\beta_1^2-j\epsilon_1)\right] \end{array} \right\|$$

where

$$D = 1-\beta_1^2-\beta_2^2 + K^2(\beta_1\beta_2+\epsilon_1\epsilon_2) + j\left[\epsilon_1-\epsilon_2+K^2\epsilon_1\beta_2(\beta_1-\beta_2)\right]$$

$$\beta_n = \frac{\omega_n}{\omega_o} \quad , \quad \omega_o = \frac{1}{\sqrt{LC_T}}$$

$$\epsilon_n = \frac{\omega_n}{\omega_c} \quad , \quad \omega_c = \frac{1}{RC_T}$$

The on-resonance transducer gain equation ($Y_{11} = Y_{22} = 0$) was then derived for a parametric upconverter (see Appendix II) with the following result:

$$G_T = \frac{4\left(\omega_2 \frac{\Delta C}{2}\right)^2 \, Re[Y_g] \, Re[Y_L]}{D^2 \left[Y_g Y_L^* - \frac{\omega_1 \omega_2 \left(\frac{\Delta C}{2}\right)^2}{D^2} \right]^2}$$

Similarly, the on-resonance gain derivation of a circulator-coupled, reflection-type parametric amplifier yielded (See Appendix III for derivation):

$$G_T = \left| \frac{-G_0 + n^2 \left[G_1 + Y_{11} - \frac{\omega_1 \omega_2 \left(\frac{\Delta C}{2}\right)^2}{D^2 \left[Y_2 + Y_{22} \right]} \right]}{+ G_0 + n^2 \left[G_1 + Y_{11} - \frac{\omega_1 \omega_2 \left(\frac{\Delta C}{2}\right)^2}{D^2 \left[Y_2 + Y_{22} \right]} \right]} \right|^2$$

In order to achieve broad bandwidths, it is first necessary to tune out the Y_{11} and Y_{22} circuit reactances. This is accomplished by simply resonating these elements at the desired frequency. However, the parametric amplifier's frequency sensitivity is primarily dependent upon the series resonance within the diode caused by the lead inductance and the junction capacitance, C_0. It is responsible for the appearance of the term D. Thus, in spite of all reactances (excluding ω_0) having been eliminated, gain over

broad bandwidths is still not constant, but slopes steeply from one edge of
the band to the other.

A study of the gain equation indicated that the effect of D could be
counteracted by using not the constant values of G_g and G_L, but rather
appropriately sloped ones. More specifically, networks were designed for
both the input and the output circuits so that

These networks were to perform essentially as equalizers whose driving-
point admittances, as seen by the varactor diode, have the prescribed
slopes. The equivalent circuit of the paramp, including the synthesized
idle network, is shown in Figure 4-2.
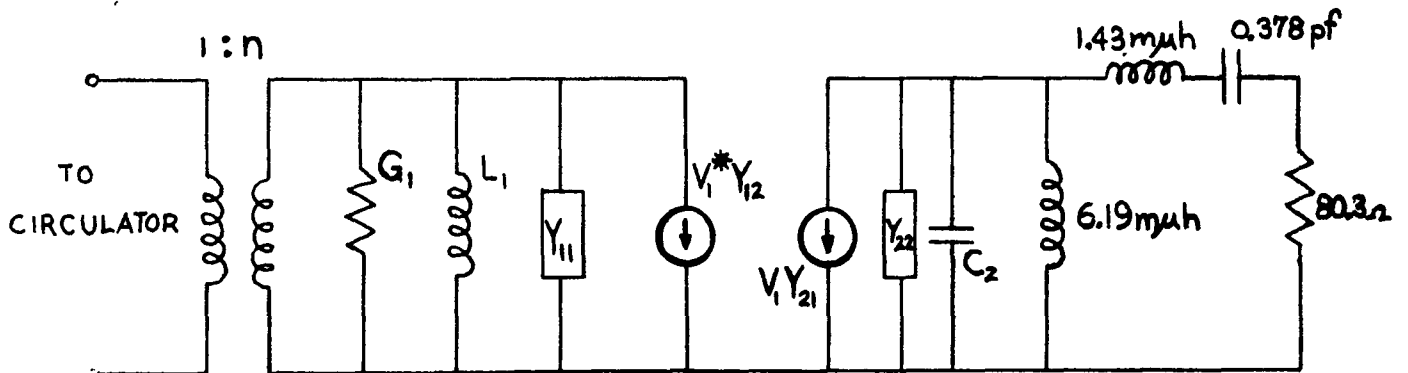
Figure 4-2. Parametric Amplifier Network

The theoretical gain variation with this network is similar to a single-tuned response with a peak gain of 11.2 db, and a 3-db bandwidth of 495 mc. Similar networks for the parametric upconverter have yielded a gain of 9.0 db and a 3-db single-tuned bandwidth of 560 mc. Measurements were made on the various RCA and Microwave Associates Diodes in order to obtain accurate diode characteristics for incorporation into the signal and idle networks. These measurements yielded fair correlation with the manufacturer's data, with the diode lead inductance always being somewhat larger. The network synthesis approach was eventually abandoned in view of the extreme difficulties of simulating lumped element networks by means of distributed elements, particularly over broad frequency bands. In addition, the theory required a high-impedance line in the vicinity of the diode (for shunt loading), which could not be accomplished without adding a diode-holder, hence additional parasitic elements.

A parallel effort was investigated during the initial phases of the contract which was an extension of the earlier (1959) work at RCA, and which culminated in a 13%-bandwidth, "L"-band paramp with 13 db of gain. Two structures were built to evaluate this mode of operation. The first unit was an all-waveguide structure, with a waveguide low-pass filter forming the diode mount. The basic drawback here was the ability of the signal waveguide to propagate the pump and idler frequency as a higher order mode. Attempts to eliminate the TE_{no} modes were not too successful, and the leakage through the low-pass filter was excessive. A possible solution might have been a doubly-corrugated, waveguide low-pass filter. The design of such filters is not always a straightforward matter. In view of this, and because of the

bulkiness of the all-waveguide structure, attention was turned to other types of structures.

The second design used a coaxial input line with a pill varactor diode in the reduced-height (RG-52/U) waveguide diode mount. The amplified output appeared at the idler frequency. Experiments showed, however, that the interaction between the pump and the signal was weak, and little gain was observed. This type of diode mount also had the disadvantage of requiring impedance transformers because of the reduced height. The latter units, with their fixed design frequencies and limited bandwidths, made this structure quite inflexible. As a result, efforts were subsequently discontinued on the reduced-height diode mounts.

This minor parallel effort led to a theoretical and experimental evaluation of existing RCA "L"-band paramps which enabled the engineer to formulate basic rules and concepts for the development of extremely broadband paramps. The results of this effort are given in Chapters III and IV.

CHAPTER II. BALANCED COAXIAL STRUCTURE

The balanced coaxial structure, originally developed by the Airborne Instruments Laboratory, has the outstanding advantage of being simple mechanically and electrically (Figure 4-3). A balanced pair of pill diodes must be used, but because of the relative directions of the idler voltages developed in the diodes, there is, ideally, no idler leakage into the signal line. This eliminates the need for blocking filters.

Considerable effort was spent in experimenting with this approach. It was felt that the structural simplicity of the mount held good promise for broadband operation. Two mounts of slightly different dimensions were built and evaluated. In the first structure the pump waveguide was RG-52/U, which has a cutoff frequency of 6.56 kmc. This size was selected because initial calculations placed the diode self-resonance, f_o, at 5 kmc, in which case the entire idler band would have been below cutoff. It should be noted that in this approach the idler frequency is placed at the self-resonance of the diode in order to achieve a minimum loading (R_s only) in the idler circuit. Since subsequent diode measurements cast some doubt on the above value of f_o, another mount having a pump line in RG-91/U was fabricated in order to be absolutely certain that no idler would leak out into the pump circuit (and contribute to the idler loading).*

With the idler adjustments largely restricted to varying the idler frequency and selecting the diodes, some adjustment must be provided in the

- -

* It was eventually found that the self-resonance of the diodes used did, indeed, fall close to 5000 mc.
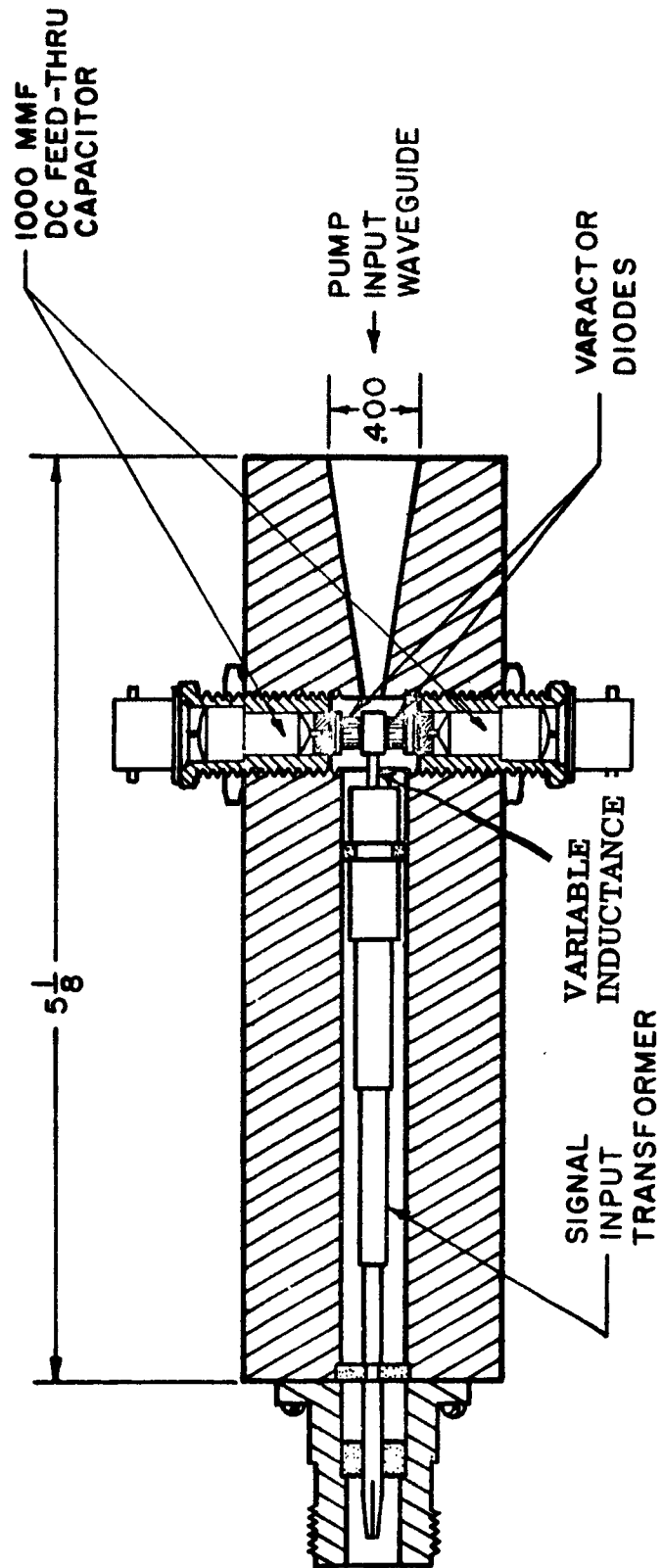
BALANCED COAXIAL DIODE MOUNT

FIGURE 4-3

signal circuit. Here a number of coaxial step transformers, intended to
counteract the combined static capacitance of the two diodes, were built and
evaluated, some of them featuring a series inductance. The impedance level
required in the input circuit was calculated to be 15 ohms; but, as mentioned,
transformers of other impedance values (5 ohms) were tried also. In addition,
a straight 50-ohm center conductor was fabricated to make measurements of
the diode impedance while the latter was in the mount. An external d-c bias
was applied independently to both diodes.

The diodes used in these experiments involved three matched pairs of
Microwave Associates pill varactors, MA4253 and MA4256 type, with C_o ranging
from $0.5\mu\mu f$ (f_c = 130 kmc) to $2.1\mu\mu f$ (f_c = 64 kmc).

The results obtained with the balanced coaxial diode mount did demon-
strate the broadband capability of the device. Thus a low gain of less than
6 db throughout a bandwidth of 2000 mc was observed at one time (Figure 4-4),
but this result was difficult to repeat. Furthermore, one half of the above
gain-bandwidth occurred outside the range of the circulator (3000-4000 mc)
used in the test. It represents, therefore, a somewhat anomalous result.
Gains as high as 23 db were also observed, but at a greatly reduced bandwidth
($<$ 10 mc). The main difficulty experienced with the balanced approach was
twofold. In the first place the device tended to be quite unstable, oscil-
lating even at low pump-power levels, long before any stable gain was evident.
Secondly, the results stated above were very critical functions of bias
voltage and pump tuning. The latter fact was probably due to the
narrow bandwidth of the pump circuit.

Two probable reasons for the inadequate performance
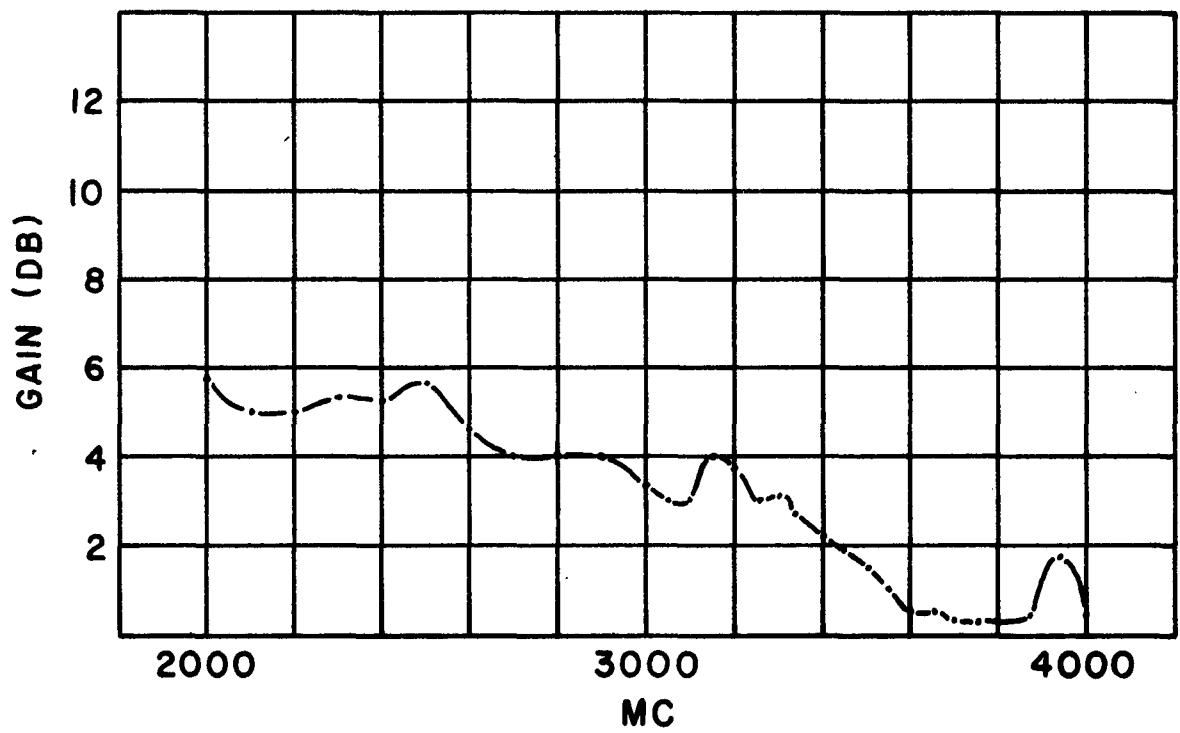
FIGURE 4-4. EXPERIMENTAL GAIN CHARACTERISTIC
OF BALANCED COAXIAL PARAMETRIC
AMPLIFIER

the shape of the coupling aperture feeding the pump power to the diodes, and the effects of the upper sideband (f_s + f_p) energy propagating in the structure. Attempts were made to adjust the coupling of the pump by means of additional tuning screws, but with limited success. Similarly, an upper-sideband filter was placed in the pump line, adjacent to the diode mount. Again, the change had little effect on the over-all performance, although it should be noted that the position of this filter is important, and that in our case this condition (an open circuit at the diode as seen by the sum frequency) most likely was not fulfilled.

Finally, there remains the possibility that, in spite of precautions taken, the losses in the structure, especially in the feed-thru capacitors for the external d-c bias, may have been excessive.

In spite of these unfavorable results, work on the balanced diode mount was continued until a parallel development produced a single diode structure promising a much better performance.

Before proceeding to the detailed description of this technique, it is worthwhile to describe some measurements made on the MA pill varactors. These measurements were undertaken using the balanced coaxial structure with the input step transformer replaced by a straight 50-ohm center conductor. The object of the study was to find out how closely the assumed equivalent circuit of the pill diode (Figure 4-5) corresponded to the actual physical unit.
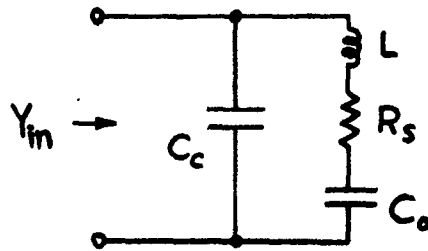
Figure 4-5 Equivalent Circuit of Pill Varactor Diode

For this purpose the Y_{in} for a pair of two MA4253 diodes was computed, using
element values supplied by the manufacturer:

$$C_c = 0.2 \mu\mu f,$$

$$L = 0.8 \ m\mu h,$$

$$C_o = 1.30 \mu\mu f,$$

$$R_s = 1.86 \ ohms$$

, The input admittance, Y_{in}, of the two diodes in parallel at the end of
the input line was then measured. Figure 4-6 illustrates the reasonably
good correlation obtained. The observed difference in the values of B/Y_o is
not too surprising when one considers the sensitivity of Y_{in} to small changes
in the parameters (L, R_s, C_c, and C_o), and the relative uncertainty of some
of the element values given. It is interesting to note that the self-
resonance of the diode does, indeed, fall near 5000 mc as initially computed.

In general, then, the balanced paramp has a signal circuit which is
adjusted to resonate at the signal frequency. That is, the inductance of the
input line and the intrinsic series resonance of the two varactor diodes
forms a net series resonance tank at the signal frequency. The input coax-
ial signal circuit employs a 50-ohm-to-15-ohm transformer to match the 50-ohm

FIGURE 4-6.

MEASURED AND CALCULATED $\left(\frac{Y}{Y_o}\right)$ OF TWO MA4253 DIODES IN PARALLEL

(Z_o = 50 OHMS)
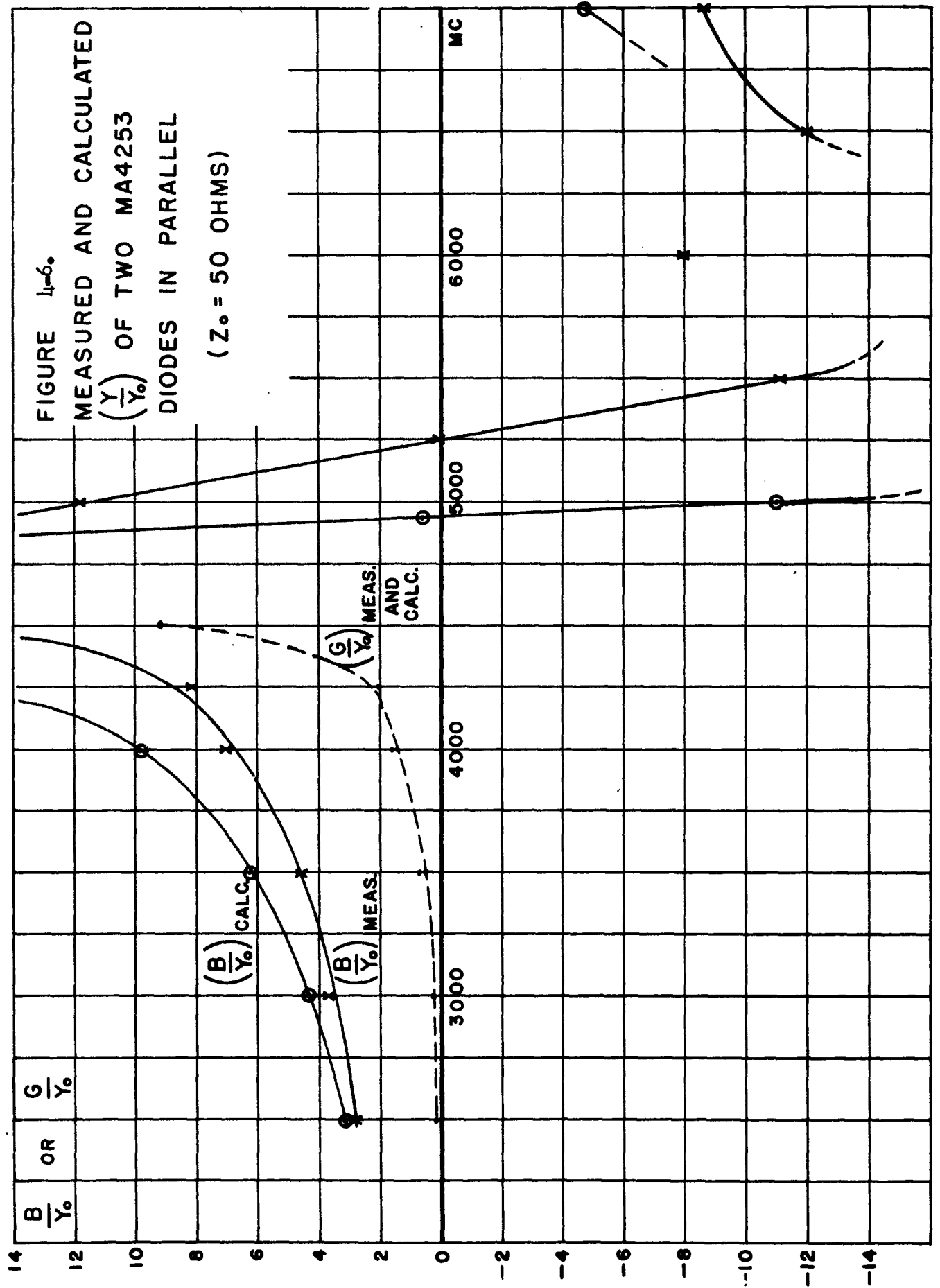
coaxial circulator to an impedance level of 15 ohms, calculated on the basis of an assumed equivalent circuit of the amplifier and given diode parameters (MA4253 diodes having $C_0 = 1.3$ pf and a cutoff frequency of $f_c = 130$ kmc). For high gains and narrowed bandwidths, an input impedance line of 7 ohms was used.

The idling circuit is made to be resonant at the natural resonance of the varactor diodes connected in series, which is equal to the resonance of a single diode for a matched pair, i.e. $W_0 = W_s = \sqrt{\dfrac{1}{LC_0}}$. Idle-circuit loading is provided by the losses inherent in the varactor diodes, and is typically equal to 2 R_s for a matched pair of varactors. It is important to note that the idling circuit cannot propagate in the pump circuit, since pump energy is coupled to the diodes through a waveguide which is beyond cut-off at the idling frequency. Also, idling currents cannot flow in the input coaxial line, since the idling voltages are in phase and add at the Y junction of the coaxial line and diode mount (hence balance).

Unfortunately the RCA balance-type paramp was very sensitive to variations in the VSWR of the input circuit as seen by the diodes. Therefore work was concentrated on the single diode approach.

CHAPTER III. SINGLE-DIODE CIRCULATOR-COUPLED STRUCTURE

It has been pointed out in a preceding section that, theoretically at least, it is possible to design networks for the input-output circuits of a parametric device which would tune out the spurious reactances present and also transform the impedances to the values required to yield the desired gain over broad bandwidths.

Although these networks have yielded excellent theoretical gain-bandwidth products, they are often difficult to realize at high microwave frequencies where inductances and capacitances must be simulated by distributed elements. Moreover, the sections of transmission line coupling the individual network elements to the varactor diode are highly frequency sensitive, which renders the exact realization of lumped element networks at microwave frequencies a difficult task, especially over broad (20 - 50%) bandwidths.

The first step in realizing broadband parametric amplifiers is to tune out the circuit and diode reactances at both the signal and idle frequencies. The signal circuit can be made to resonate at the natural frequency of the varactor, the bandwidth of this circuit being determined by the transformed generator conductance and case capacitance. The case capacitance must always be less than C_o by at least a factor of two. The natural resonance of the input circuit is determined by noting the rectified voltage level caused by the diode barrier resistance as a function of input frequency. Elementary circuit theory shows that the voltage across the capacitance is a maximum at series resonance for an RLC circuit. (It is not true for inductance.) Since the self-resonant frequency of the diode is placed at the input signal frequency, the diode at the idling frequency appears inductive. The addition

of a waveguide external capacitance, C_x, (not seen by the coaxial signal circuit) resonates the idling frequency at the desired frequency.

These observations have led to a criterion which has great applicability in the design of broadband parametric amplifiers.

The method depends on the maximum utilization of the parasitic elements (R_s, L, C_o, C_c) of the varactor diode, plus certain simple experimental techniques which are easily applied. As an illustration of the power of this method, some results obtained with the S-band device using both modes of operation, circulator-coupled and upconverter, are shown in Figure 4-7. A complete gain characteristic for the 830-mc bandwidth case is shown in Figures 4-8 and 4-9. A typical gain characteristic for the amplifier, in which high gain over a narrower bandwidth is shown, is illustrated in Figure 4-10.

The technique is best explained by noting that it is possible to define a transmission characteristic for a varactor diode which is a function of the elements L, R_s, C_o, C_c of the diode, and whose precise definition and functional relationship depend on the manner in which the diode is used in the circuit.

Let us consider a typical input circuit of a parametric amplifier. In its basic form, it is a transmission line, terminated by the varactor diode (Figure 4-11). A transformer is added which permits the adjustment of the generator impedance as seen by the diode. The other parameters shown are as follows:

L = diode lead inductance,

C_c = case capacitance,

	CIRCULATOR - COUPLED			UP CONVERTER
GAIN	9.5 db	20db	10db	14.5 db
BANDWIDTH	830 MC	330MC	370MC (B 0.4db)	400 MC
NOISE FIGURE	≈2.1db	NOT MEASURED		≈1.5 db

S - BAND PARAMETRIC AMPLIFIER EXPERIMENTAL RESULTS

FIG. 4-7.
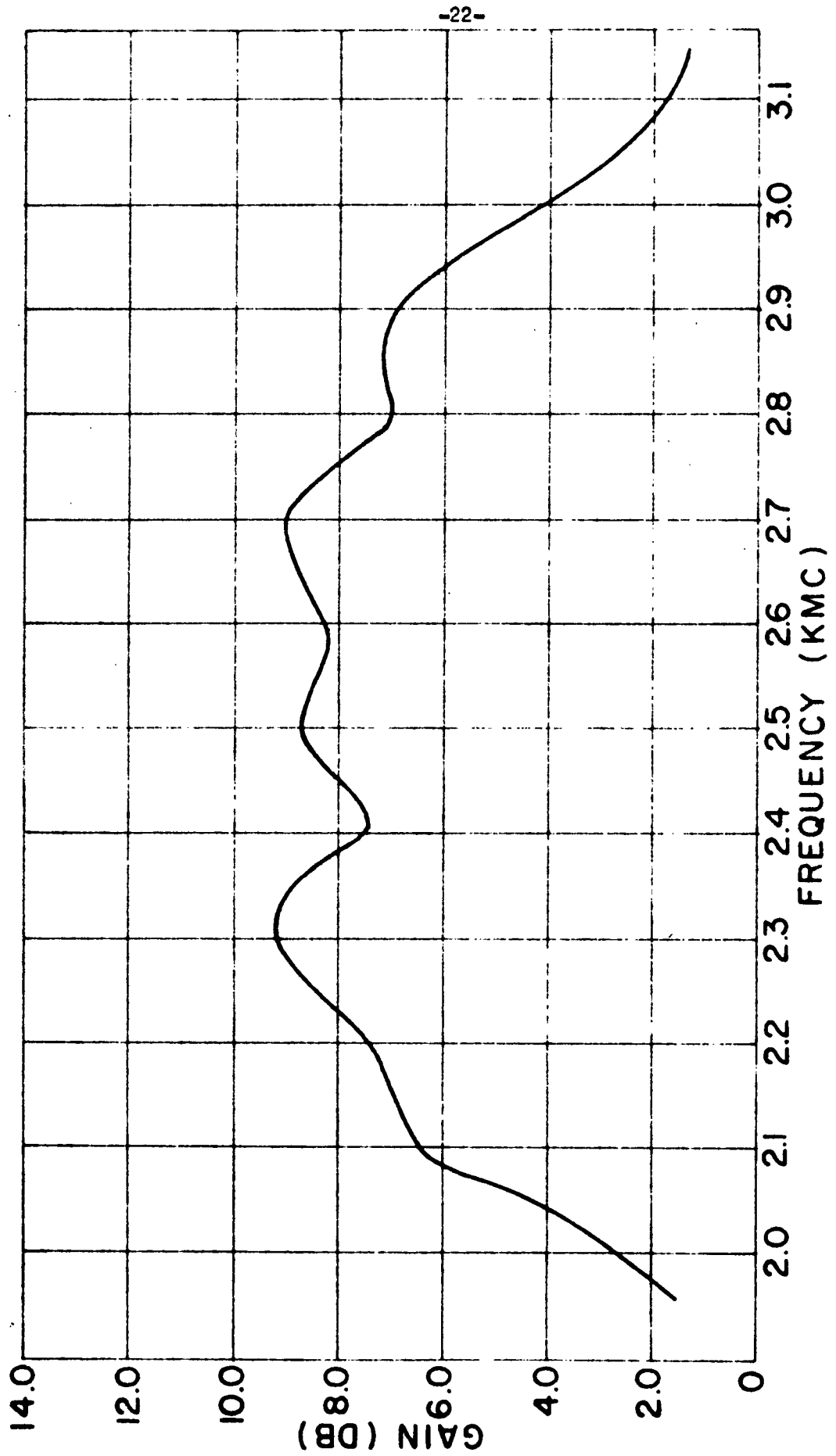
Figure 4-8. GAIN RESPONSE OF BROADBAND PARAMETRIC AMPLIFIER

Figure 4-9.
FREQUENCY RESPONSE
WIDE BAND
PARAMETRIC AMPLIFIER

FIGURE 4-10.
GAIN-BANDWIDTH RESPONSE FOR
SINGLE DIODE NON-DEGENERATE
PARAMETRIC AMPLIFIER
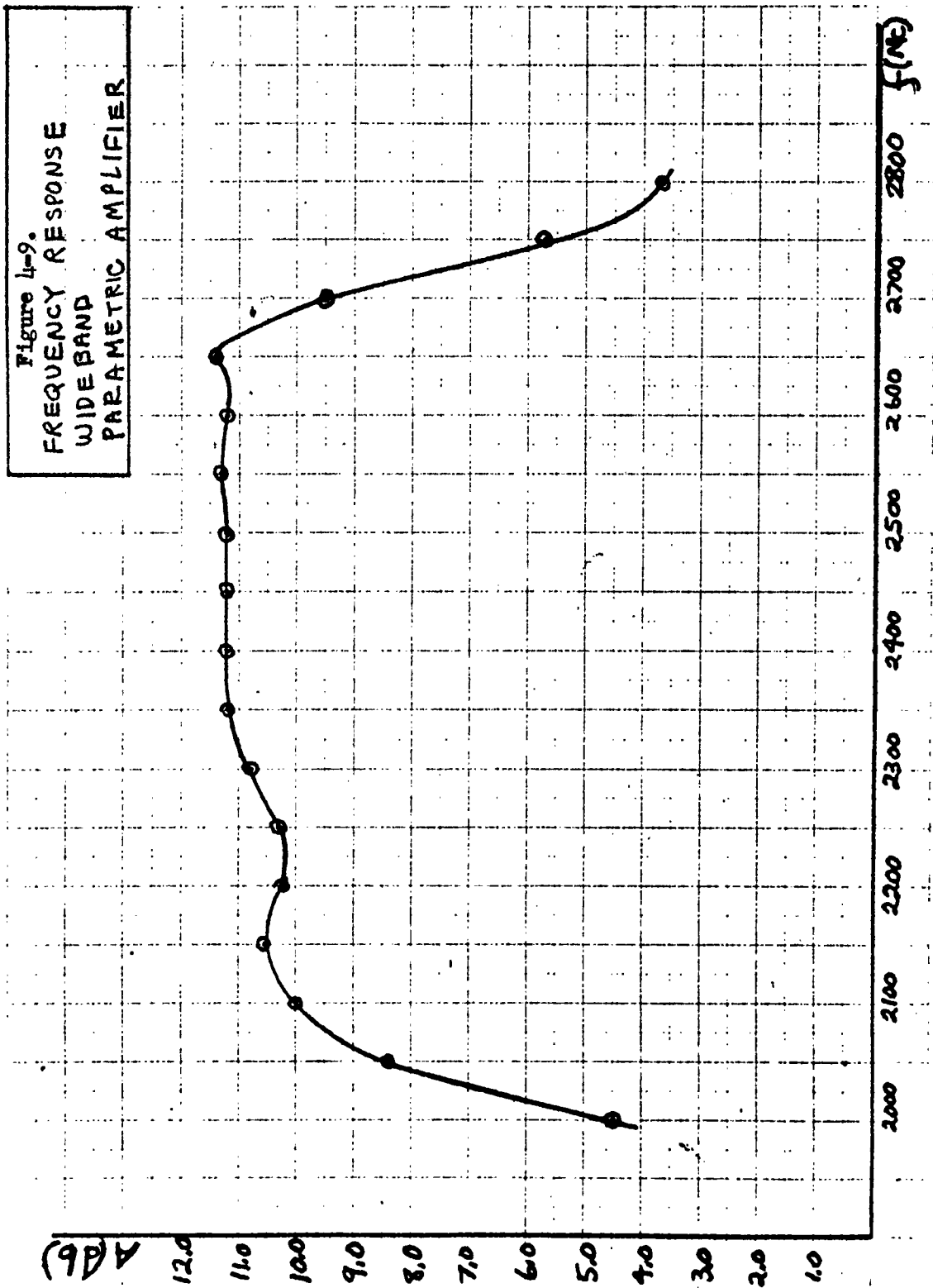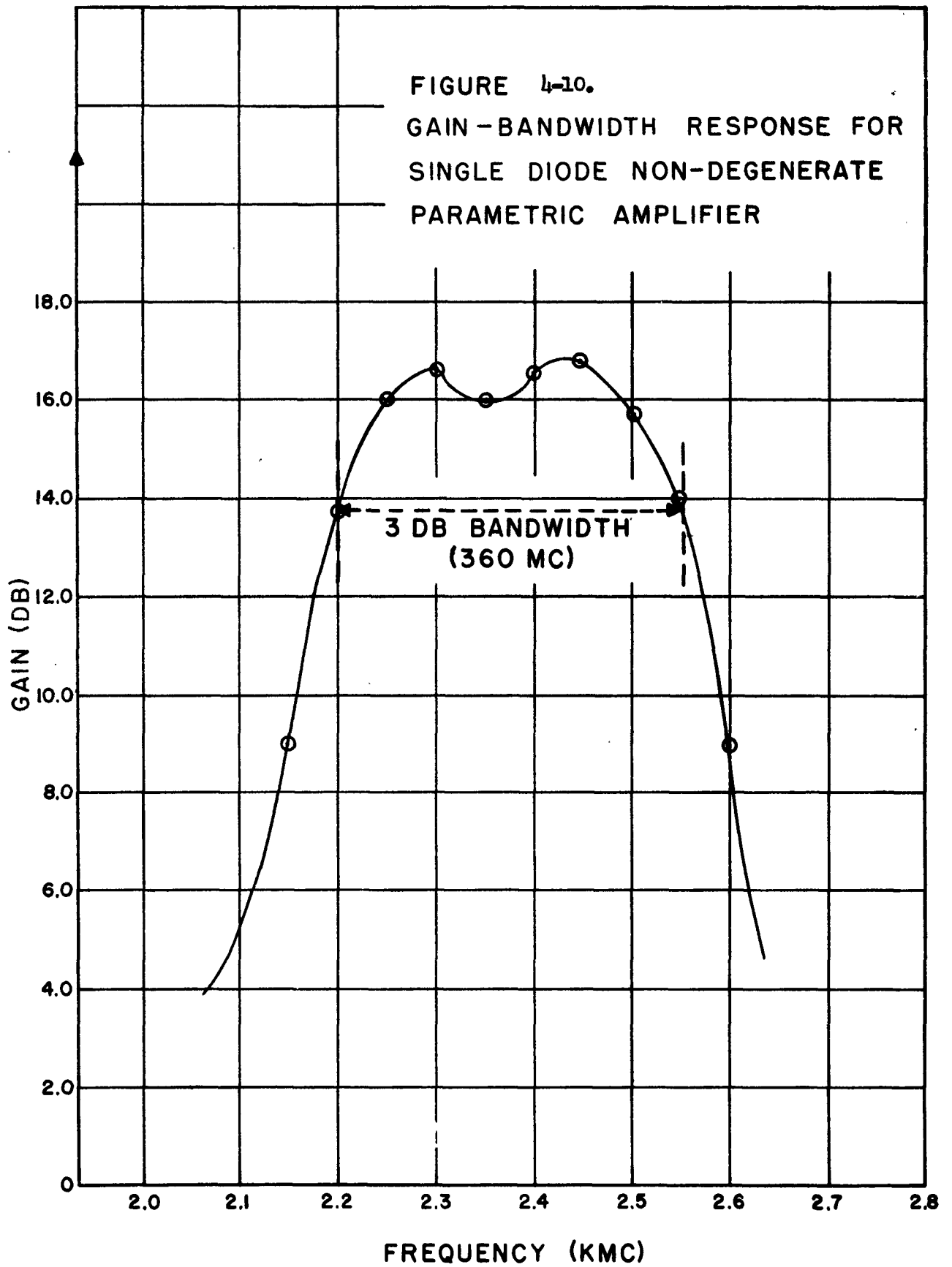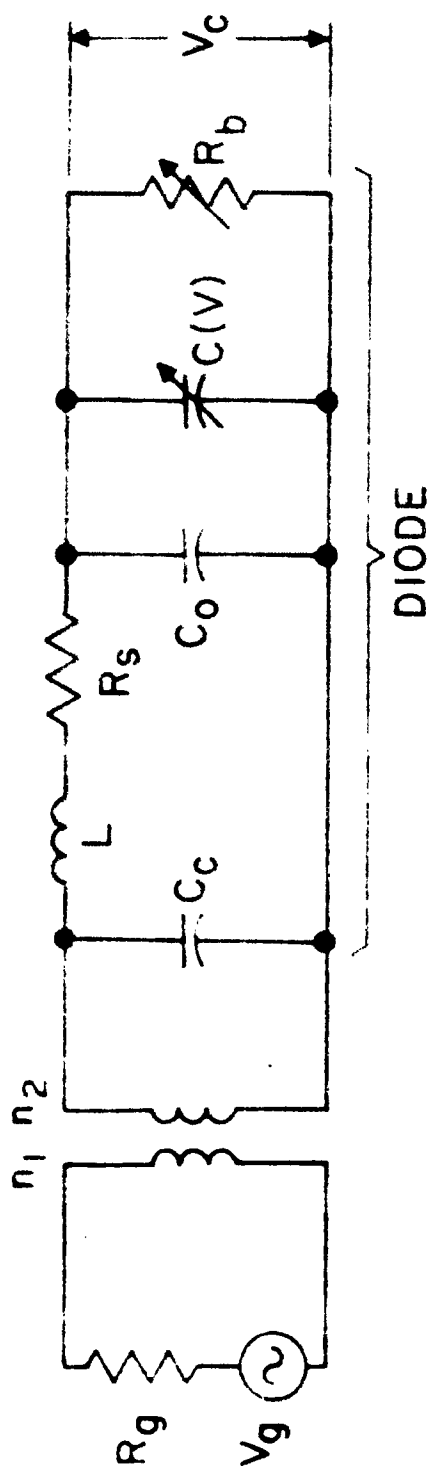
VARACTOR DIODE TERMINATING THE INPUT LINE

$$\left|\frac{V_c}{V_g}\right| = \frac{\left(\frac{n_2}{n_1}\right)}{\left[1-\left(\frac{\omega}{\omega_0}\right)^2 - \omega^2 R_g' R_s C_0 C_c\right]^2 + (\omega C_0)^2\left[R_s + R_g'\left[1+\frac{C_c}{C_0}\left(1-\left(\frac{\omega}{\omega_0}\right)^2\right)\right]\right]^2}$$

$$\omega_0^2 = \frac{1}{LC_0}$$

$$R_g' = \left(\frac{n_2}{n_1}\right)^2 R_g$$

Figure 4-11.

C_o = junction capacitance at bias point,

$C(v)$ = capacitance variation caused by the pump,

R_s = spreading resistance of the diode,

R_b = non-linear barrier resistance (very high in the backward direction),

R_g = input resistance of the signal source.

The quantity of interest is now the ratio V_c/V_g as a function of frequency and of the diode parameters. This can be looked upon as a ratio of the measure of transmission of the input voltage to the variable capacitance. It can be expressed by the equation shown in Figure 4-11, where the parameters of special interest are the transformer ratio n_2/n_1, and the self-resonant frequency of the diode, f_o. Figure 4-12 shows some results of calculations based on the above equation, using typical values for the diode parameters:

R_g = 50 ohms,

R_s = 2.0 ohms,

C_o = 1.0,

C_c = 0.4,

L = 2.0 mh,

f_o = 3560 mc.

As expected, the dependence of V_c/V_g on frequency and loading (i.e., on R'_g) is that of a tuned RLC circuit.

The significance of Figure 4-12 is that by choosing the self-resonant frequency, f_o, and the transformer ratio, n_2/n_1, one is able to control the transmission of the input voltage to the variable capacitance $C(v)$. Given a
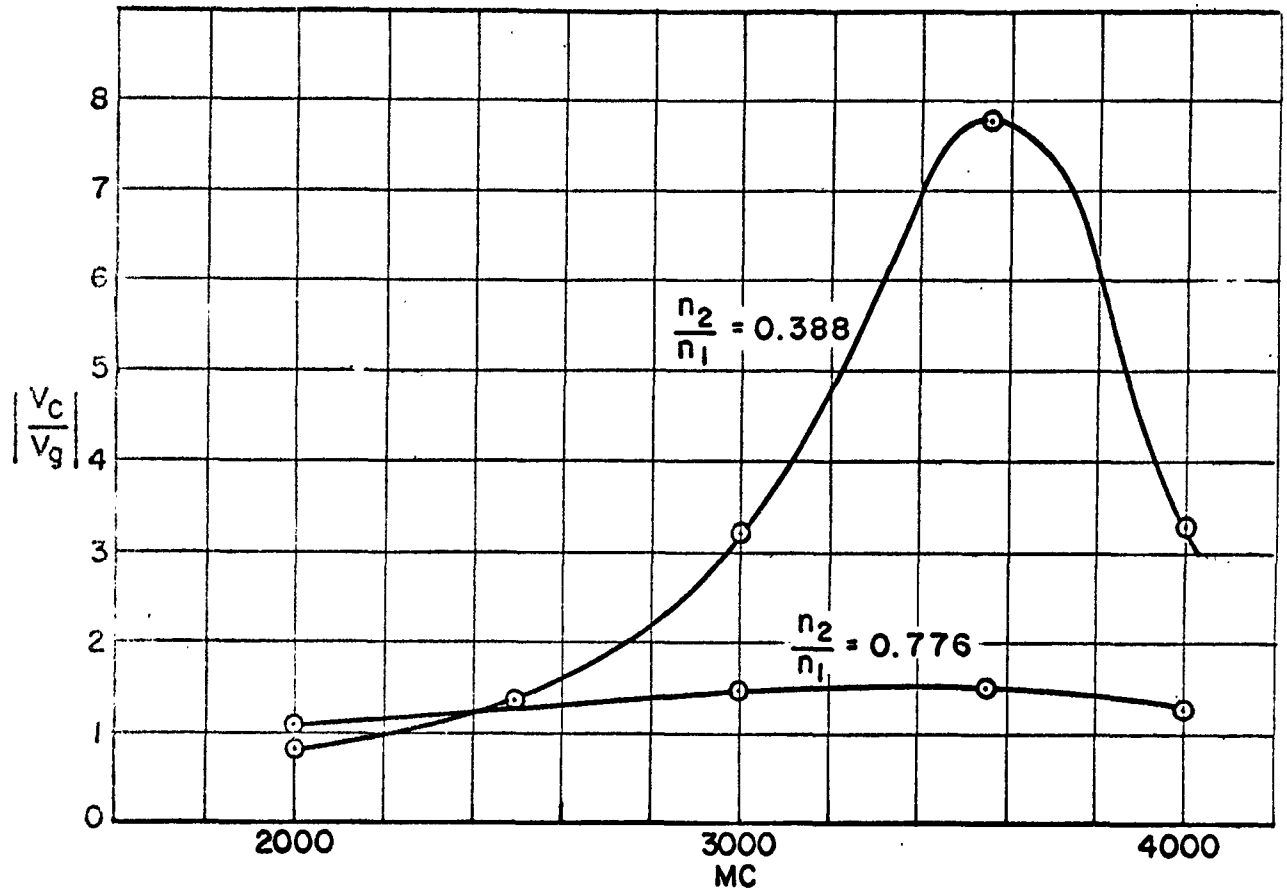
FIGURE 4-12. $\left|\dfrac{V_C}{V_g}\right|$ AS A FUNCTION OF TRANSFORMER RATIO

certain band of signal frequencies, it is thus possible to obtain the most
efficient transmission over the given band to ensure a maximum interaction
between the signal and the pump at frequencies of interest. It should be
noted at this point that the above technique requires placing the self-
resonance of the diode at the given signal frequency of the device.
Further adjustments can then be made by altering the transformer ratio, and
to a lesser extent by adjusting the bias voltage.

In an actual development, one need not depend on theoretical calcu-
lations alone. The voltage, V_c, can be determined experimentally by observ-
ing the rectified output of the diode while sweeping the input signal over a
band of frequencies (Figure 4-13). Since rectification is caused by the non-
linear barrier resistance, R_b, maximum rectification implies a maximum
voltage across the variable capacitance (Figure 4-11). More accurate results
are obtained by measuring the d-c output with a sensitive voltmeter, while
keeping the input power constant at all frequencies. The resultant data
then represents the quantity k V_c/V_g, where k is a constant. In Table I,
below, these data are shown for several diodes, illustrating the differences
from unit to unit.
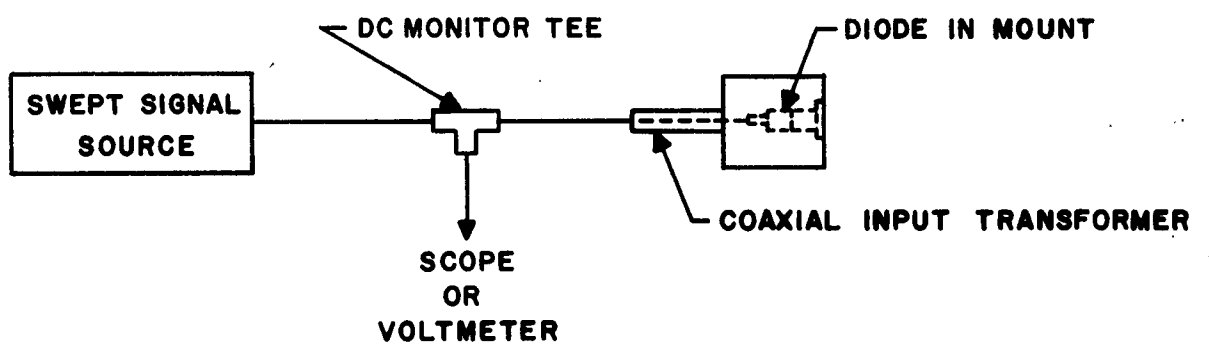
FIGURE 4-13. EXPERIMENTAL CIRCUIT FOR MEASURING $K \left| \dfrac{V_c}{V_g} \right|$.

TABLE I - SAMPLE DATA ON k V_o/V_g OBTAINED WITH VARIOUS DIODES

Freq. (mc)	#1 MA460E	#2 MA450ER	#3 SX106P	
2000	0.585	0.235	0.400	
2200	0.492	0.167	0.700	
2400	0.590	0.045	0.560	
2600	0.215	0.019	0.900	All data in volts
2800	0.252	0.036	1.280	
3000	0.226	0.026	1.290	
3200	0.091	0.009	1.390	
3400	0.079	0.006	0.580	
3600	0.058	0.004	0.420	
3800	0.060	0.004	0.300	
4000	0.022	0.002	0.160	

Appendix IV contains all the data for those diodes tested during this program.

Figure 4-14 shows some experimental results obtained by the above technique. The input was kept constant at 1 mw at all frequencies. As seen from the plot, the measured curves resemble those calculated from the equation in Figure 4-11. Two transformers were used, with R'_{g1} = 20 ohms, and R'_{g2} = 7 ohms. As expected, the 7-ohm transformer yields a sharper response.

A noticeable discrepancy between the calculated and the measured results should be pointed out at this time. If one calculates the self-resonant frequency, f_0, using the known values of L and C_0, the result (and hence the location of the calculated peak of V_o/V_g) may be significantly higher than
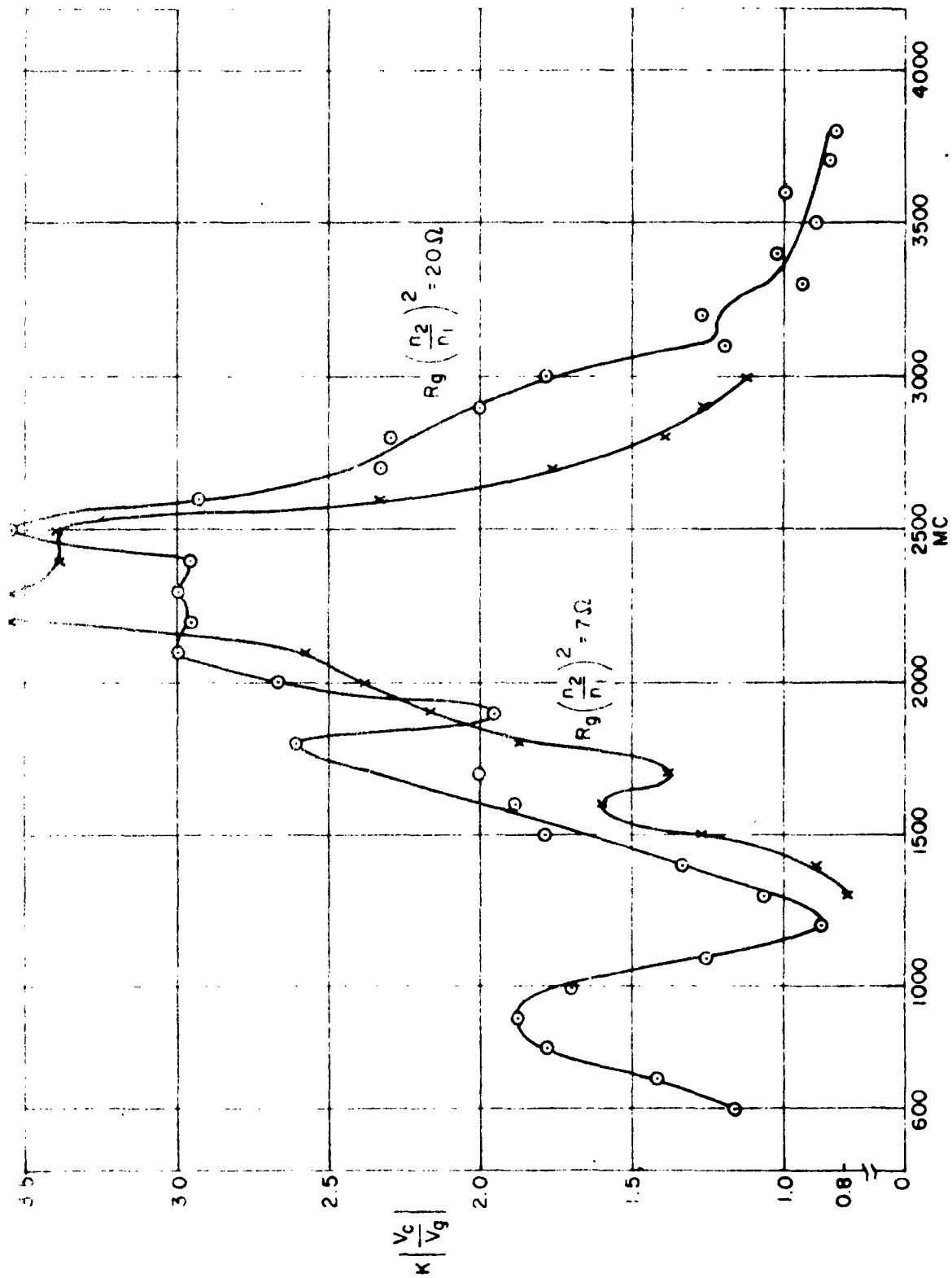
FIGURE 4-14. EXPERIMENTAL RESULTS FOR $K\left|\dfrac{V_c}{V_g}\right|$

the frequency at which the measured peak occurs. One possible reason is that the input power level employed to observe rectification, i.e., the input voltage swing, may cause a sufficient capacitance variation to change the effective C_o. This is so because the curvature of the C vs. V characteristic causes the capacitance variation to be distorted even while the pumping voltage is sinusoidal. Another reason could be the fact that the results calculated in Figure 4-12 are based on the equivalent circuit shown in Figure 4-11, where the barrier resistance, R_b, was assumed to be very high (the diode in its backward region). During the flow of forward current, R_b is quite low, eventually decreasing to near zero for large forward voltages. This change in the network parameters may cause a redistribution of voltage drops across the individual elements.

Although the exact cause for the discrepancy has not been fully explained, the basic argument regarding the desirability of a maximum voltage transmission at the frequencies of interest still holds. In all cases tried, a good transmission of the input voltage was the key to satisfactory performance of the device. The technique can, therefore, be used to rapidly check the diodes at hand, and to find the unit best suited for the intended application.

The situation in a typical idler circuit of a parametric amplifier is somewhat different. With the idler frequency commonly placed at high microwave frequencies (X-Band, for example), the structure consists of a varactor diode usually shunt mounted across the waveguide (Figure 4-15). A transmission characteristic for this structure is now defined in the conventional two-port sense (i.e., one can measure either the VSWR or the insertion loss

COAXIAL INPUT LINE

SHORT SECTION
OF WAVEGUIDE

DIODE IN MOUNT

SWEPT FREQUENCY
INPUT

LOAD FOR VSWR
MEASUREMENTS OR
DETECTOR FOR
INSERTION LOSS
MEASUREMENTS
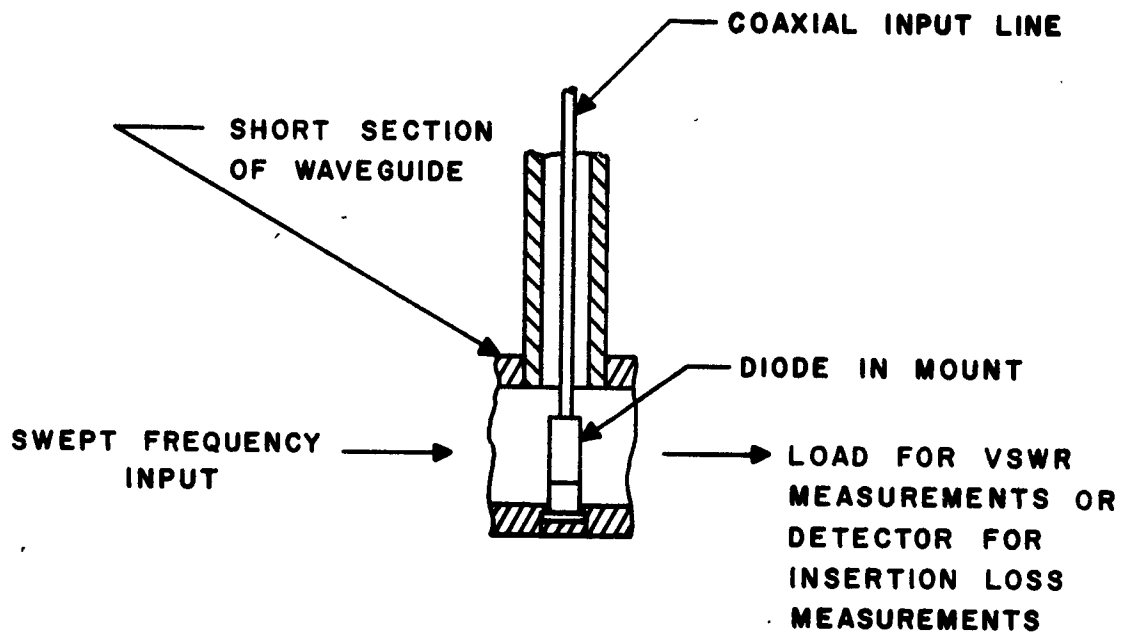
FIGURE 4-15. METHOD FOR DETERMINING PASSBANDS
IN THE IDLER CIRCUIT.

of the diode-mount combination). It has been found that this combination does exhibit a characteristic which is generally of the bandpass type. The most significant fact is that the extent and the location of the passband can be controlled by varying the following:

    (a)   the type of diode, i.e., essentially the elements of the diode;

    (b)   the type and the size of the structure holding the diode;

    (c)   the bias voltage applied externally.

Figure 4-16 illustrates this dependency on the type of obstacle used (i.e., basically the geometry of the mount), while Figure 4-17 does the same for varying bias voltage. It should be mentioned that a similar phenomenon has been described by DeLoach, who showed that a Bell Laboratories' Sharpless type diode, mounted in a capacitive transverse ridge, has a bandpass characteristic.

This characteristic is easily measured by plotting the VSWR and/or the insertion loss of the diode-mount combination. An input swept over the idler frequency band can be utilized to expedite the work. It has thus been possible to find diode-obstacle combinations which exhibit extremely broad (over 1000 mc at X-Band) bandpass type responses.

The exact equivalent circuit of such a diode-obstacle combination in waveguide is difficult to derive. A reasonably accurate representation of a diode mounted in a partial height post is shown in Figure 4-18, where L_p and C_p denote the inductance and the capacitance of the post, respectively. Since at frequencies higher than f_o the diode is inductive, the observed bandpass characteristic appears to be due to a broad resonance between C_p and the inductance formed by the diode.
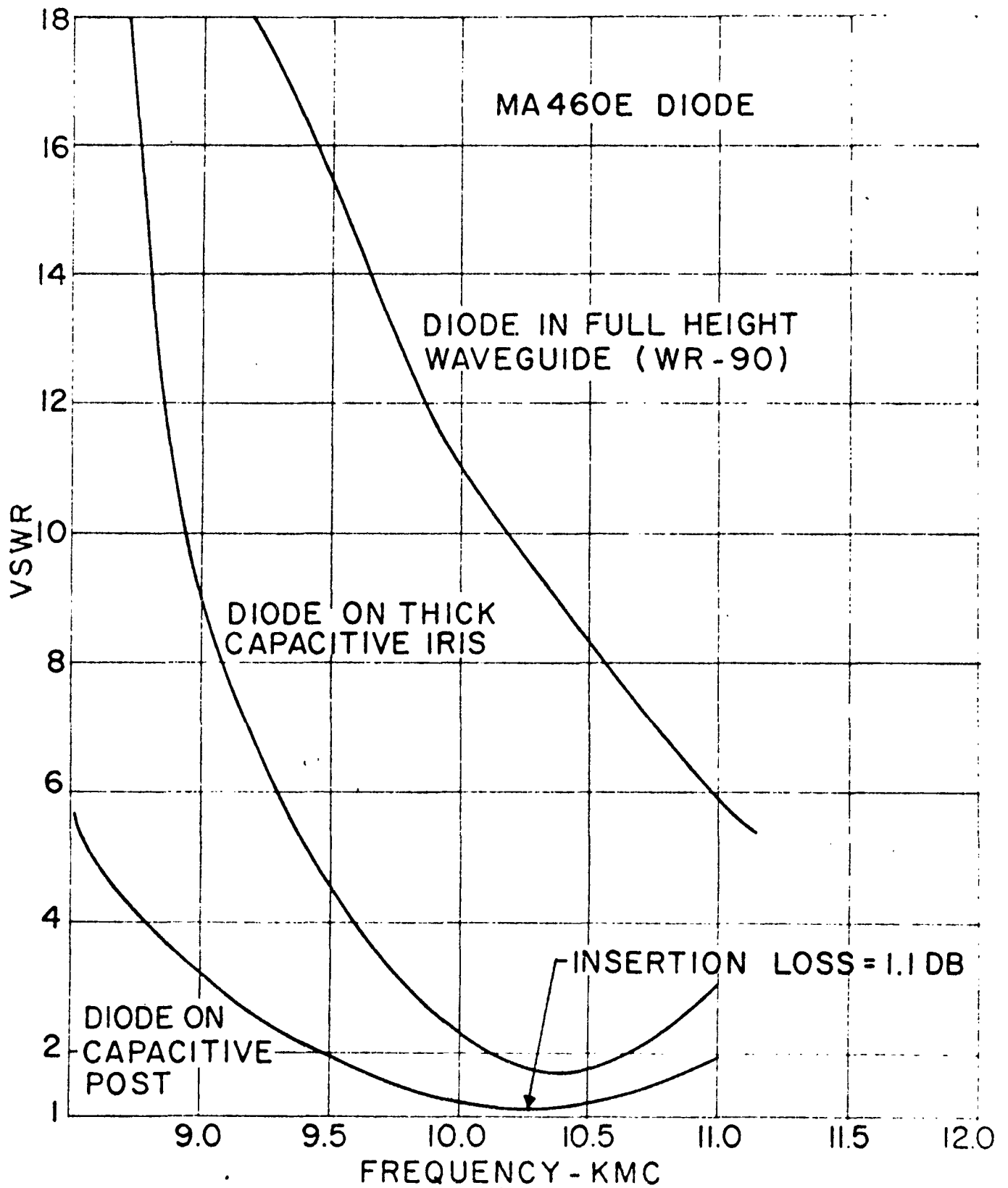
FIG. 4-16.   EFFECT OF OBSTACLE ON DIODE PASSBAND
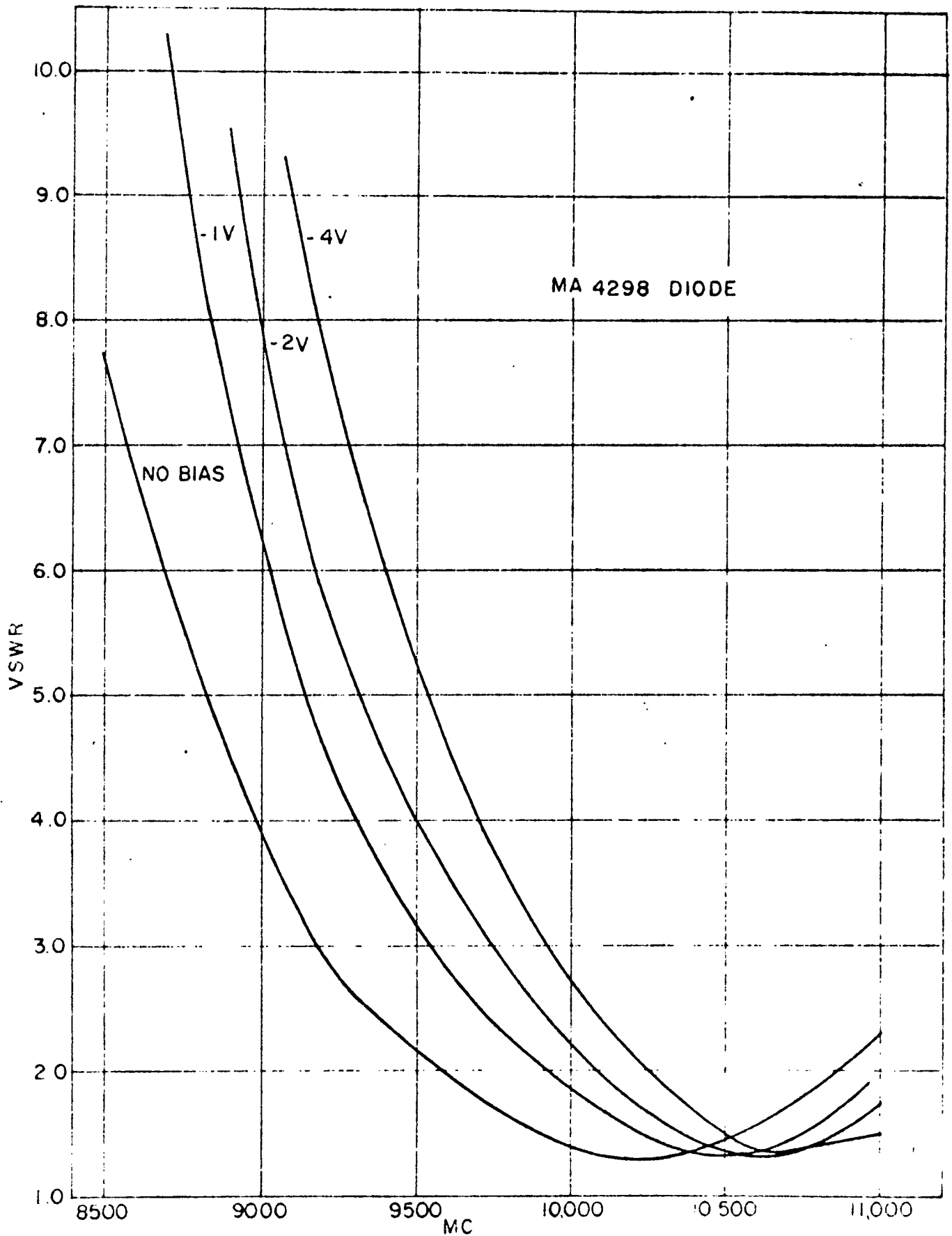
FIGURE 4-17. EFFECT OF BIAS VOLTAGE ON DIODE PASSBAND
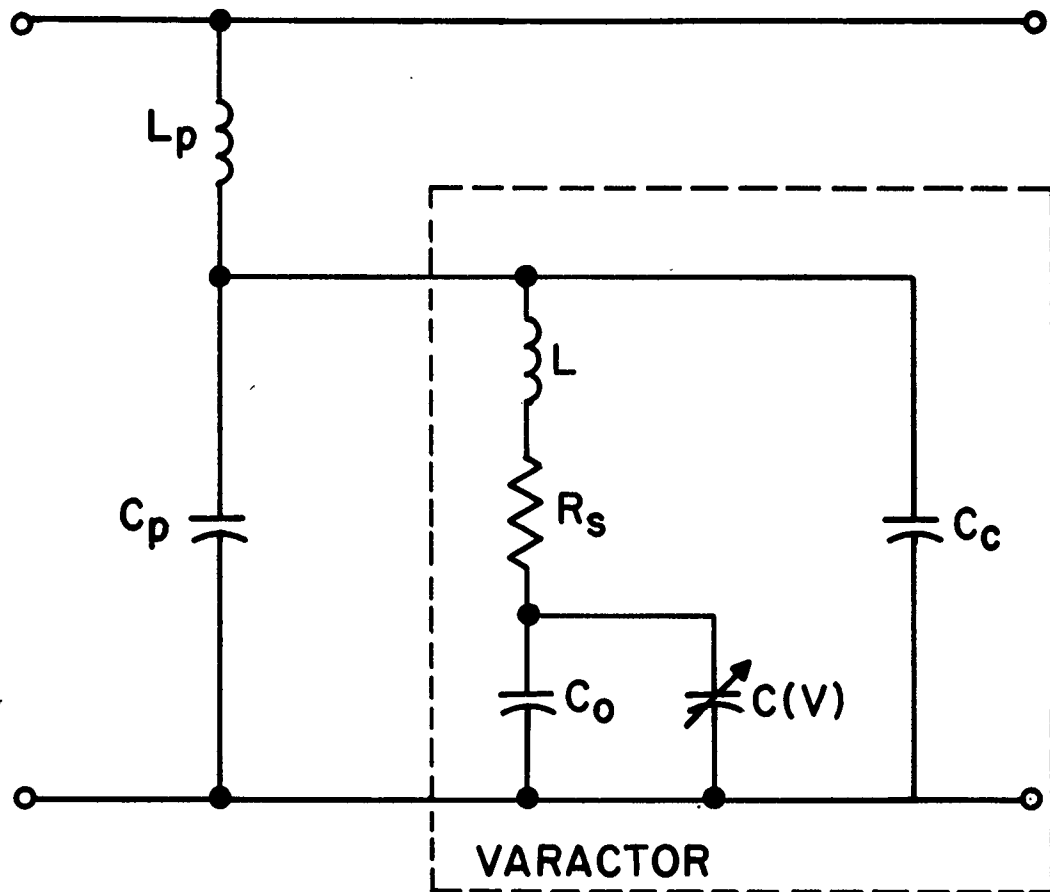
Figure 4-18.

EQUIVALENT CIRCUIT OF VARACTOR DIODE
MOUNTED IN AN ASYMMETRICAL POST

The significance of the transmission characteristics and passbands just described lies in the fact that by operating the parametric amplifier within the bands of maximum transmission, large gain-bandwidth products can be achieved. It has been possible to develop single-channel (non-degenerate) gain-bandwidth products approaching 3300 mc (Figure 4-7). Several reflection-type parametric amplifiers have yielded 2-5 db of gain over the full octave bandwidths i.e., from 2000 mc to 4000 mc.

It should also be noted that by placing the pump frequency outside the observed idler passband, little leakage of pump into the idler circuit occurs, and there is no need for a filter to block the pump. This results in a simpler structure and eliminates the extra length of line that the filter introduces.

A broad signal-circuit passband was achieved by series resonating the varactor diode. A broad idle-circuit passband was achieved by resonating the diode susceptance, which was primarily inductive, with the capacitance of a partial bright post built into the waveguide mount. This capacitive post does not appreciably affect the signal circuit, since the diode mount will not permit waveguide propagation at the signal frequencies.

In conclusion, it is felt that the above technique, utilizing the inherent transmission bands of the diode and the mount, represents a useful criterion which allows the designer of a parametric amplifier to make a better evaluation of the various structures and diodes at hand. Since the gain of a parametric device is a function of many variables, such as Δ C, line impedances (i.e., the loading), losses in the circuit, etc., the existence of passbands at the operating frequencies is not a sufficient condition for

optimum performance. Their existence does, however, appear as a necessary condition, especially in breadband applications.

CHAPTER IV. OTHER EXPERIMENTAL RESULTS

The breadband input circuit of the paramp has been used in conjunction with a narrow-band-idling, resonant-box circuit in order to achieve rapid electronic tunability by simply varying the pump frequency. No other adjustments are necessary. Typical results are as follows:

Signal Frequency	Pump Frequency	Idle Frequency	G	BW
3.1 GC	12.4 GC	9.3 GC	16 db	60 mcs
2.96	12.3	9.34	16	65
2.91	12.24	9.33	16	60
2.78	12.14	9.36	17	70
2.70	12.07	9.37	16	60
2.65	11.89	9.24	16	60
2.60	11.84	9.24	17	70
2.55	11.78	9.23	16	60
2.50	11.70	9.26	16	60
2.45	11.58	9.13	16	60
2.40	11.55	9.15	16	80
2.30	11.475	9.175	16	60
2.25	11.38	9.13	16	60

Other tunable results have been obtained with a gain of 30 db and instanteous bandwidth of 5 to 10 mc. It must be pointed out that this experiment is by no means optimum, since the pump frequency could not be raised above 12.4 Gc, and the pump high-pass filter cut off at 11.30 Gc. More recent experiments have shown that tunable paramps can be built to cover a 2000-mc

bandwidth at S-band.

Mechanically Tuned Paramp

The idling circuit of the paramp can be represented as shown below,
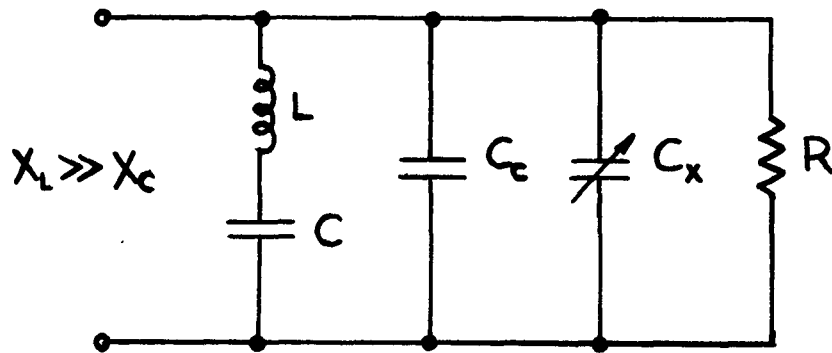
Figure 4-19 Paramp Idler

where C_X is a variable-capacitance ridge whose variation is determined by a screw position. The capacitive reactance of the ridge is plotted in Figure 4-20. The ridge capacitance determines the shunt idle resonance; thus, broad tuning ranges are possible without altering the pump frequency. The paramps could be tuned over a 900 mc range, with the instantaneous gain-bandwidth product varying from 145 mc to 378 mc throughout the desired range.

Summary

A simple experimental technique has been developed which permits the construction of single-diode parametric amplifiers and upconverters capable of high gain-bandwidth performance. The technique is based on the fact that a very-broadband over-all circuit is possible if the self-resonance of

Figure 4-20.	TITLE IMPEDANCE vs. OFFSET FOR RG 58/U WG	DWG. NO.
FORM 82BSPR (2-49)	KAY ELECTRIC COMPANY, PINE BROOK, N.J. ©1949 PRINTED IN U.S.A.	DATE

IMPEDANCE OR ADMITTANCE COORDINATES

RADIALLY SCALED PARAMETERS
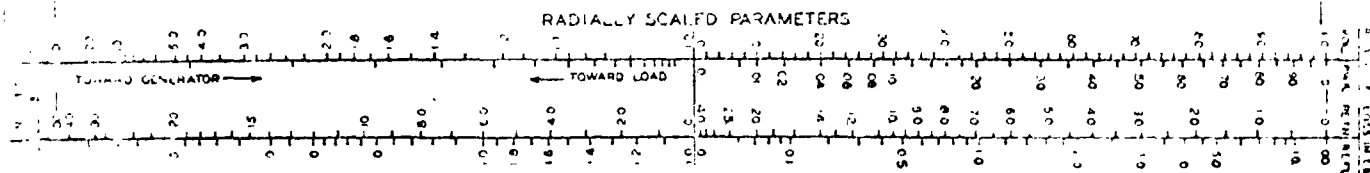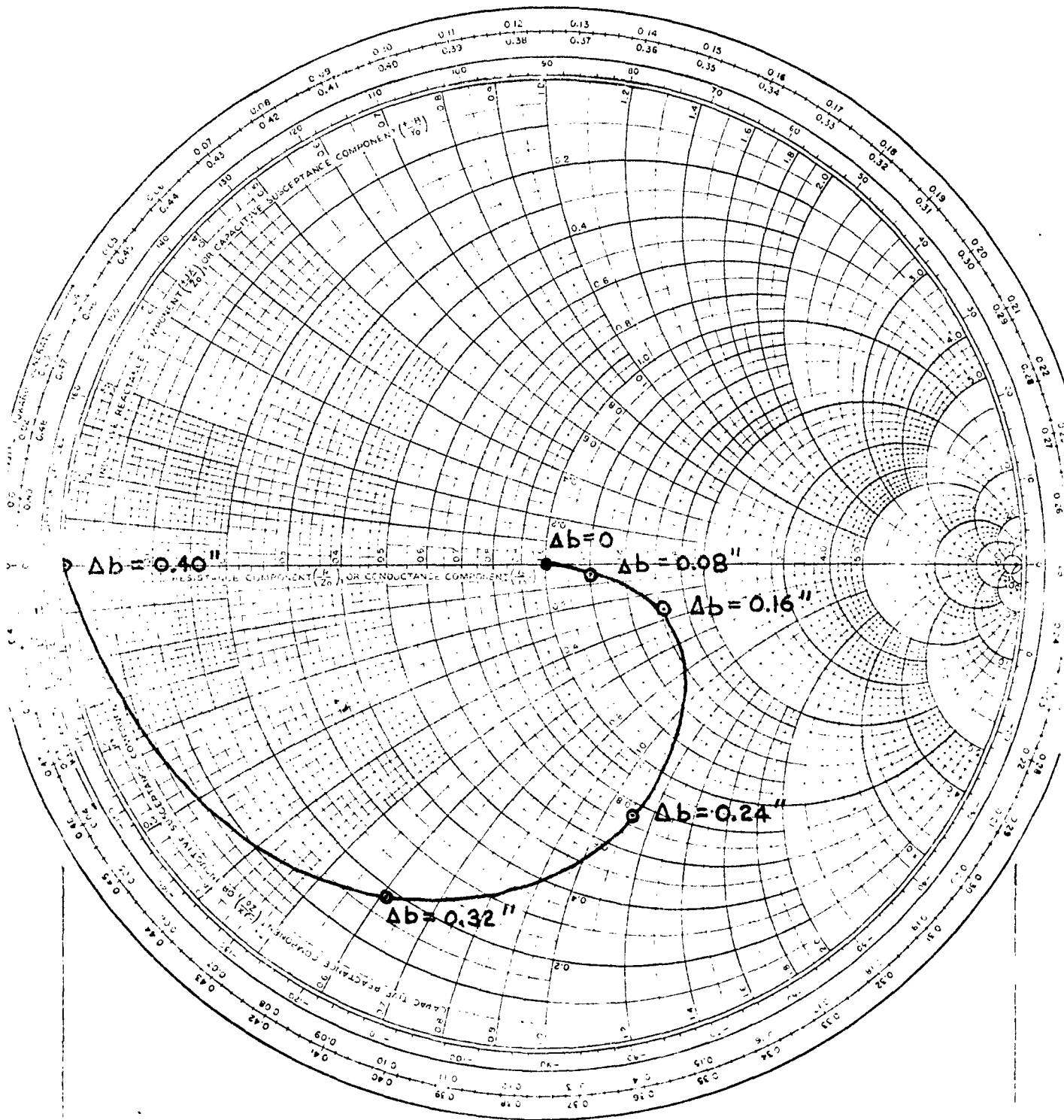
the diode is placed at the input frequency, while a combination of the diode and a suitable waveguide obstacle is resonated at the idler frequency. Two easily-applied experimental tests are described for evaluating and optimizing the signal and the idler circuits. In the first test the rectification of the diode in its mount is measured at the specified input frequency and the circuit is adjusted for maximum rectified output. This ensures a maximum input-signal voltage across the variable capacitance, $C(v)$, of the diode under actual operating conditions. In the idler circuit the test consists of measuring the VSWR of the diode-obstacle combination. The latter is then adjusted until a broad passband is obtained at the idler frequency.

It has been found that the above two tests lead to a necessary condition for broadband operation. Several non-degenerate parametric amplifiers have been built using this principle. Voltage gain-bandwidth products of 3300 mc have been achieved at S-band.

The stability of the paramp is excellent. For example, pump power variations of 2 db will alter the gain response by less than 1 db. Pump frequency variations of 30 mc will affect the gain response by 1 db. An ambient temperature rise of $25^{\circ}C$ will not affect the paramp bandwidth but will decrease the gain by 0.7 db.

The extremely broadband paramps (30 to 40% bandwidths) require hand-picked diodes at this time. For example, 19 Microwave Associates varactors were tested with capacitance tolerances of 40%. Two diodes were capable of 30 to 40% instantaneous bandwidths (> 10 db gain). All 19 diodes yielded a minimum of 15% bandwidth (>10 db gain).

CHAPTER V. ALTERNATE COUPLING METHODS

Although circulators are available to cover the frequency bands 2-3 kmc and 3-4 kmc, it is advantageous to consider other possible coupling schemes in this program. This section describes several techniques for coupling the signal into the broadband filter-parametric diode configuration and extracting the amplified output. These techniques include direct, hybrid, upconverter and circulator coupling schemes, and are applicable to either the degenerate or non-degenerate modes of operation. Although the degenerate mode of operation was not considered on this program, it is mentioned here as a means of comparing potential operation of the device in either single or double-sideband receivers.

In the degenerate mode of operation, the signal and idle bands coincide, whereas in the non-degenerate mode they occupy separate regions of the frequency spectrum. An input spectrum, $\triangle f$, produces an inverted idle spectrum, $\triangle P$. In the non-degenerate mode, operation extends over $2\triangle f$ (signal plus idle band) to provide an effective amplifier bandwidth of $\triangle f$. However, in the degenerate mode, operation extends only over $\triangle f$, since the signal and idle bands coincide; hence the effective bandwidth is $1/2 \triangle f$. A 2.0 kmc input band centered at 3 kmc provides an effective amplifier bandwidth of 1.0 kmc in the degenerate case. In addition to the bandwidth limitation, degenerate mode operation is normally inferior to non-degenerate mode operation in terms of noise figure. In single-channel operation, the minimum amplifier noise figure is 3 db, since the signal and idle noise components both contribute equally to the over-all signal noise power. This noise figure can be reduced somewhat by utilizing a synchronous pumping scheme, although the tech-

nical problems involved do not normally justify the improvement. The idle

noise in the non-degenerate amplifier, however, is reduced by the factor

$\frac{W_1}{W_2}$, as it is coupled to the signal channel; hence noise figure levels much

below 3 db are achievable. In both modes of operation, the over-all gain is

due entirely to regeneration (as contrasted to the upconverter, paragraph d,

where conversion gain contributes to the total gain, thereby improving its

stability). The several schemes which may be used to couple to the basic

amplifier configuration are discussed below.

a.   Direct-Coupled Amplifier

This mode of operation is one in which the input and output frequencies

are equal and appear at the same port. The apparent noise figure[1], F', for

this device is:

$$F' = 1 + \frac{G_1}{G_g} + \frac{G_L}{G_g} + \frac{G \ W_1}{G_g \ W_2} \ , \qquad (5\text{-}1)$$

where

G_g = Input Conductance

$\frac{G_1}{G_g}$ = Noise Contribution from Circuit and Diode Losses

$\frac{G_L}{G_g}$ = Noise Contribution of Load

- -

1. Apparent noise figure, F', is a modified definition of conventional noise
    figure to include the effect of load noise. Hence, from an application
    viewpoint, it provides a more meaningful figure of merit than does the
    conventional definition, which excludes load noise.

G $\qquad$ = Negative Conductance of Amplifier

$\dfrac{W_1 \, G}{W_2 \, G_g}$ = Noise Contribution from Idle Circuit

It is evident from equation (5-1) that the contribution of load noise and idle noise to the amplifier noise figure is reduced by light output coupling $\left(\dfrac{G_L}{G_g} \ll 1 \right)$ and wide separation of the signal and idle bands $\left(\dfrac{\omega_1}{\omega_2} \gg 1 \right)$. In order to achieve stable gain and minimum frequency sensitivity, it is desirable that $\dfrac{G_L}{G_g} \sim 1$. Thus the direct-coupled scheme would provide a minimum noise figure of 3 db for a lossless paramp (noise figure = 0 db). This approach is, therefore, not to be too highly considered. The effect of load noise can be eliminated by means of the hybrid coupler or ferrite circulator, as each serves to isolate the load from the amplifier input.

b. Hybrid-Coupled Amplifier

The hybrid can be utilized to couple to a parametric amplifier as shown in Figure 4-21.

ω_P

1

3

PARAMP

2

IDLE

4

OUTPUT

A

SINGLE DIODE PARAMP

IDLE

1

3

2

4

ω_P

IDLE

B

DUAL PARAMP
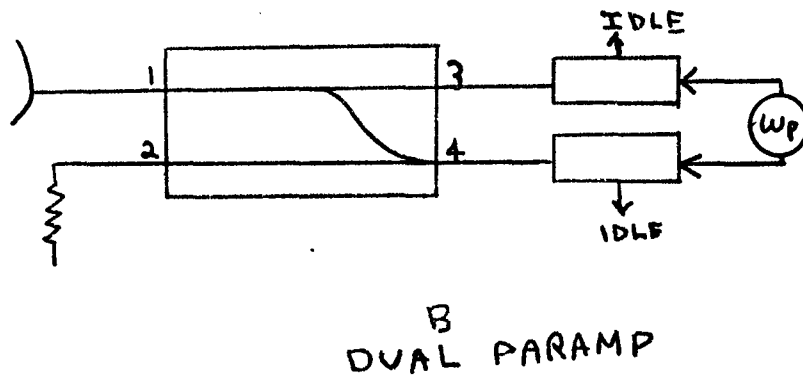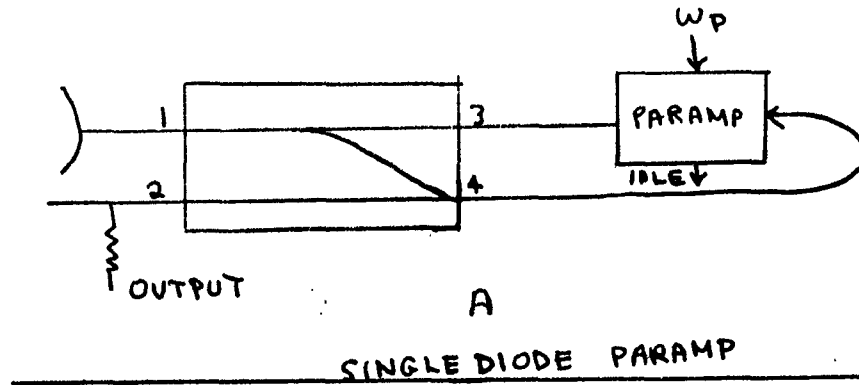
Figure 4-21. Hybrid-Coupled Amplifier

An input at port 1 will split equally in magnitude and 90° out of phase to the identical amplifier stages and be amplified. The resultant amplified signals will add in phase in arm 2, out of phase in arm 1 and, hence, couple completely to port 2. Consequently, the entire output appears at the load. In the same way, noise or reflections from the load are amplified and coupled entirely to port 1. Hence, noise isolation of the load is achieved. The amplifier apparent noise figure is:

$$F = 1 + \frac{G_1}{G_g} + \frac{W_1}{W_2} \frac{G}{G_g}$$

In the absence of parasitic losses, and for high gain, the noise figure is approximately: $F = 1 + \frac{W_1}{W_2}$ and, hence, is primarily determined by the ratio of signal to idle frequency. In the degenerate case, $W_1 = W_2$; consequently, the minimum noise figure is 3 db (lossless paramp). Operation in the non-degenerate mode, of course, will result in lower values of amplifier noise figure.

Since the system must exhibit moderately-high regenerative gain, it is important that a good match exist at each port, and that the isolation of the hybrid coupler be high. If ρ is taken as the isolation between two adjacent arms, and also as the reflection coefficient at all terminals, then the stability conditions become $G_A \rho^2 < 1$, where G_A is the regenerative gain of each amplifier stage. For a 13-db amplifier gain and a 6-db margin against oscillation, $\rho^2 < 1/4 \times 1/20$. Hence, the VSWR at all connections must be less than 1.25 and the coupler isolation greater than 19 db over the input band. RCA-New York was the first to utilize the hybrid scheme in the development of octave-bandwidth tunnel-diode amplifiers. The disadvantages of using the hybrid scheme are listed below:

1. More pump power required for a given gain.

2. Arms 3 and 4 of the hybrid must remain balanced at all times.

3. The load must have a near perfect match (VSWR = 1.1) over the entire band of frequencies to be amplified. Any mismatch at the load will cause a feedback loop to the paramp and cause instability and oscillation.

c. Circulator-Coupled Amplifier

Due to the non-reciprocal nature of the circulator, noise arising at the load is isolated from the amplifier stage and is transmitted instead to a matched termination. Thus, the apparent noise figure can be expressed as:

$$F' = 1 + \frac{G_1}{G_g} + \frac{W_1 \, G}{W_2 \, G_g} \, .$$

As in the hybrid-coupled scheme, the minimum noise figure for degenerate mode operation is 3 db (lossless paramp). Lower noise figures can be achieved in the non-degenerate mode.

d. Lower Sideband Upconverter

The feasibility of providing a filter-type parametric amplifier with 13-db gain over an octave bandwidth is primarily dependent upon the techniques employed in synthesizing the idler and diode networks, since the diode parasitic elements (particularly self-resonance) introduce frequency-sensitive terms in the over-all gain expression, which greatly deteriorates the amplifier performance. These detrimental effects can be somewhat alleviated by using multiple-cavity networks in which the diode self-admittances at the input and output frequencies are incorporated as parts of a ladder structure. In this manner, the admittances seen at the diode, looking in either direction, can be kept real over a large band of frequencies and substantial gain-bandwidth products are possible. Because of the frequency sensitive terms in G and P, the gain will not be altogether flat; yet, the basic argument for obtaining broad bandwidth still holds, since the regenerative amplification may be sloped so as to cancel these known effects.

The immediate advantage of the upconverter is that for a given amount of net gain, the amount of regeneration needed is less than in all the previous cases discussed. Therefore, an extremely-stable, low-noise amplifier may be constructed by taking advantage of conversion gain, W_2/W_1, while providing a controlled amount of regenerative, $K/(1-2)^2$, gain. The limit of conversion gain is normally determined by the succeeding downconverter stage and, hence, the output frequency.

Load isolation is an inherent property of the upconverter, since the noise arising from the load is amplified regeneratively, while the signals from the input experience regenerative plus frequency conversion, thereby improving the output signal-to-noise ratio by the factor W_2/W_1. The apparent noise figure of the upconverter can be expressed as

$$F'up = 1 + \frac{G}{G_g} + \frac{G_{T_1}^2}{GG_g} \frac{W_1}{W_2} .$$

The noise figure of this upconverter at a signal frequency of 3 kmc will be in the order of 2.2 db. One of the formidable limitations of the proposed upconverter is the necessity for a broadband downconverter. This means that the downconverter must have an information bandwidth of 2000 mc and a noise figure of 8.9 db. Tunnel-diode downconverters are definitely not recommended at this time because of their limited bandwidth under matched conditions. The noise figure of the conventional mixer can be expressed by:

$$F_{\triangle G} = 1 + \frac{20I_o}{G_g} + \frac{G_{T_1}^2}{G_g \, G_R} \, \frac{(1 + 20I_o)}{C_{T2}} \, \frac{(G_L + G_2)}{G_{T2}} + \frac{G_1}{G_L} ,$$

where

$$G_{T1} = G_{11} + G_1 + G_g,$$

$$G_{T2} = G_{22} + G_2 + G_L,$$

$$G_R = \frac{\Delta G^2}{4 \, G_{T2}} \, .$$

By assuming $\Delta G = 0.0006$ mho, the above expression yields a noise figure of 9 db, indicating a parametric-upconverter, conductance-down-converter noise figure of approximately 3.0 db.

RCA-New York has built an ortho mode type of mixer with an IF information bandwidth of 1000 mc. However, the complete 2000 mc bandwidth does not appear feasible at this time, due to the absence of proper matching networks and low-noise 2000 mc IF's.

The parametric downconverter, or demodulator, has a noise figure which can be expressed as:

$$F_d' = 1 + \frac{G_2}{G_L} + \frac{W_2}{W_1} \frac{1}{N} \qquad \text{(where } N = \frac{G}{G_g} \text{)} \, ,$$

where

$$G = \frac{4N}{(1 - N)^2} \frac{W_1}{W_2}$$

The noise figure of the downconverter stage is 11 db of a regenerative gain of 6 db (conversion loss of 7.5 db), and a net demodulator loss of 1.5 db. However, this noise figure does not include the 2000 mc IF noise figure, which will invariably raise the second-stage noise contribution considerably.

A novel type of mixer using a non-linear capacitance-conductance

characteristic, which should have a noise figure in the order of 3 to 5.6 db, is presently being analyzed by RCA-New York.

This technique is the most promising, since it offers a positive input impedance while providing regeneration and a low noise figure. To be sure, the present resistance mixers have a limited barrier-capacitance variation, which in some instances allows for a mixer noise figure less than that predicted by resistance theory. One immediate example of this is the Varian Orthomode Mixer, which has a noise figure ranging from 4.0 to 6.0 db, depending upon the selection of diodes. However, low-noise mixers can conceivably be provided by simply operating the diode in the highly non-linear conductance capacitance region (+ 0.1 volt). The noise figure expression for a diode with $\triangle C$ and $\triangle G$ variation is

$$F_{\triangle C \triangle G} = 1 + \frac{20 I_o}{G_g} + \frac{G_{T1}2 + g^2}{G_g(G_R + \frac{G_c W_2}{W_1})} \cdot \frac{(1 + 20 I_o)}{G_{T2}} \frac{(G_L + G_2)}{G_{T2}} + \frac{G_1}{G_g}$$

where

$$g = \frac{(W_2 - W_1) \triangle G \triangle C}{4 \, GT_2} \, ,$$

$$G_c = \frac{(W_1 W_2 \triangle C^2)}{4 \, G_{T2}} \, .$$

Assuming a diode with a $\triangle C = 0.466 \, 10^{-13}$ farads and a $\triangle G = 0.0006$ mho, we can expect a noise figure ranging from the optimistic lossless case of 3 db to the pessimistic loss case of 5.6 db.

e. Double Sideband Varactor Upconverter

There are three basic modes of operation of variable-reactance communications receivers. They are, respectively, the negative-resistance type, the upper-sideband type, and the lower-sideband type. The amplifier described here is one which has been investigated extensively in the RCA Microwave Applied Research Group, and which was reported on by W. Eckhardt and F. Sterzer at the International Solid State Circuit Conference in 1960. It makes use of the power output at both sidebands.

The power flow at different frequencies in a lossless non-linear reactor is governed by the Manley-Rowe equations

$$\sum_{m=0}^{\infty} \sum_{n=-\infty}^{\infty} \frac{mP_{mp+ns}}{mfp+nfs} = 0 \qquad (e-1)$$

$$\sum_{m=-\infty}^{\infty} \sum_{n=0}^{\infty} \frac{mP_{mp+ns}}{mfp+nfs} = 0 \qquad (e-2)$$

(where P_{mp+ns} is the net power absorbed by the non-linear reactor at frequency mf_p+nf_s). These equations show that double-sideband upconversion (i.e. power input at f_p and f_s, power output at f_p' and $f_p \pm f_s$) is a particularly advantageous mode of operation. If only the lower sideband ($f_p - f_s$) is allowed to exist, negative resistance is exhibited by the pumped non-linear reactor at both f_s and ($f_p - f_s$), resulting in basically unlimited gain, but also in only conditional stability. If, on the other hand, only the upper sideband exists, the pumped non-linear reactor represents a positive resistance at both f_s and ($f_p + f_s$), but the conversion gain is limited to the ratio

$\dfrac{f_p + f_s}{f_s}$. When both sidebands exist in proper proportion, however, it is

possible to combine the advantages of the two single-sideband cases, i.e., to

obtain basically unlimited yet unconditionally stable gain. This can be shown

by specializing the Manley-Rowe equations for the case in which power flows

only at the frequencies f_p, f_s, and f_{p+s} (i.e., for m, n = o, ± 1):

$$\frac{P_{p-s}}{f_p - f_s} + \frac{P_p}{f_p} + \frac{P_{p+s}}{f_p + f_s} = 0 \quad , \tag{e-3}$$

$$\frac{P_{p-s}}{f_p - f_s} + \frac{P_s}{f_s} + \frac{P_{p+s}}{f_p + f_s} = 0 \quad . \tag{e-4}$$

For $P_s = 0$, equations e-3 and e-4 assume the following forms:

$$\frac{P_{p-s}}{f_p - f_s} = \frac{P_{p+s}}{f_p + f_s} \quad , \tag{e-5}$$

$$P_p = - \left(P_{p-s} + P_{p+s} \right) \quad . \tag{e-6}$$

Equation (e-5) proves that unlimited, unconditionally stable gain is

indeed possible, because $P_s = 0$ is compatible with sideband powers > 0.

Equation (e-6) indicates that all of the sideband power leaving the non-

linear reactor (in the case of $P_s = 0$) is supplied by the pump.

Additional advantages of this type of amplifier are the freedom from

the requirement for a circulator to separate the input and output signals,

and the broad bandwidths achievable. With a 10-kmc pump, Eckhart and

Sterzer of RCA were able to achieve a gain-bandwidth product of 1.5 kmc,

using diodes which were available in 1959. In a narrower-band unit, they

achieved better than 3-db noise figure. It seems clear that with presently available diodes, and an extension of the theory to include efficient demodulator schemes, it may be possible to demonstrate extremely broad bandwidths.

CHAPTER VI. MISCELLANEOUS TOPICS

DIODES

The best results have been achieved using a cartridge-type silicon varactor diode with the following characteristics:

$$\gamma = \frac{C_1}{2C_o} = 1/6$$

Breakdown Voltage = -5 volts

C_o = 0.8 pf

Lead Inductance $\cong$ 2 nh

Cutoff Frequency $\cong$ 110 kmc (measured at breakdown)

It looks like the diode used has not exhibited an abnormally-high value of due to an anamolous minority carrier charge storage effect; however, this has not been conclusively proven.

NOISE FIGURE

It is significant that the circulator-coupled parametric amplifier displayed a reasonably-low noise figure (i.e. $\cong$ 2.1 db) despite the fact that external idler loading was employed. If a simplified equivalent circuit for the parametric amplifier is used, in which there is no external idler loading, the optimum pump frequency and noise figure can be computed from:

(7)

$$f_3 \text{ optimum} = f_1 \sqrt{1 + (\quad Q)^2} \cong \gamma Q f_1 ,$$

where

f_1 = signal frequency.

Now, letting $\gamma = \frac{C_1}{2C_o} = 1/6$ for graded junction diode, where small-signal

diode capacitance = $C = C_0 + C_1 \cos \omega_3 + \ell \, \omega_3$ = pump frequency, for a graded junction diode operated at a voltage approximately 1/2 its breakdown voltage, the cutoff frequency at the operating point will be:

$$f_c = 110 \Big/ 3\sqrt{2} = 8.7 \text{ kmc},$$

where f_c = diode cutoff frequency at the operating point.

Thus, since

$$Q = f_c \Big/ f_1 = 87 \Big/ 2.5 = 34.8,$$

f_3 optimum $= (34.8/6)(2.5) = 14.5$ kmc.

It should be noted that as the dissipation losses go up (i.e., lower diode cutoff frequency and/or external idler loading) the optimum pump frequency goes down. The actual amplifier on this program was pumped at 12.2 kmc.

At room temperature, the noise figure for this optimum condition is

$$F \text{ min} = 1 + 2 \left[\frac{1}{\gamma Q} + \frac{1}{(\gamma Q)^2} \right] ,$$

$$= 1 + 2 \left[.17 + .03 \right] = 1.40 .$$

Taking into account the loss of the ferrite circulator, the over-all paramp noise figure is

$$F = (L_1 - 1) + F \text{ min}$$

$$= 1.025 - 1 + 1.40 = 1.425;$$

for a 0.1-db loss in the circulator, $10 \log F = 1.54$ db.

Most previous effort on broadband parametric amplifiers has been restricted to the use of no external idler loading in order to achieve the optimum noise figure. Although the 2.1-db noise figure obtained on this

—

program is higher than the idealized optimum noise figure, it is quite satisfactory for most low-noise amplifier applications.

It should also be noted that all known theoretical work on noise-figure optimization has not fully taken into account the diode parasitic circuit elements (lead inductance and case capacitance), as well as the variations in circuit elements due to the mounting of the diode in a microwave transmission-line structure. Another assumption employed in all theoretical work is sinusoidal pumping. In practice, the pump swing is about 0.5 volts positive, and the pump voltage is being clipped on the forward half-cycle.

The low noise performance has been achieved using about 200 milliwatts of pump power; however, the actual pump power across the diode non-linear capacitance is somewhat less, due to dissipation losses in the pump-circuit high-pass filter and voltage division between the diode-lead inductance and the diode non-linear capacitance.

GAIN SATURATION

A typical gain-saturation curve for the circulator-coupled parametric amplifier is shown in Figure 4-22. Since a varactor diode with a breakdown voltage of -5 volts was employed, some improvement in saturation characteristics can be obtained by going to diodes having -6 volts at breakdown.

TUNING

All of the broadband performance reported on this program was for amplifiers using three X-Band (RG-52/U waveguide) slide-screw tuners in the idle circuit. A special triple-screw was designed and fabricated as a possible replacement for the three slide-screw tuners. This tuner consisted

FIG 4-22. TYPICAL GAIN SATURATION CHARACTERISTIC

f_o = 2400 MC
AMPLIFIER GAIN = 71 DB
AMPLIFIER BANDWIDTH = 250 MC

POWER INPUT
DBM

-59-
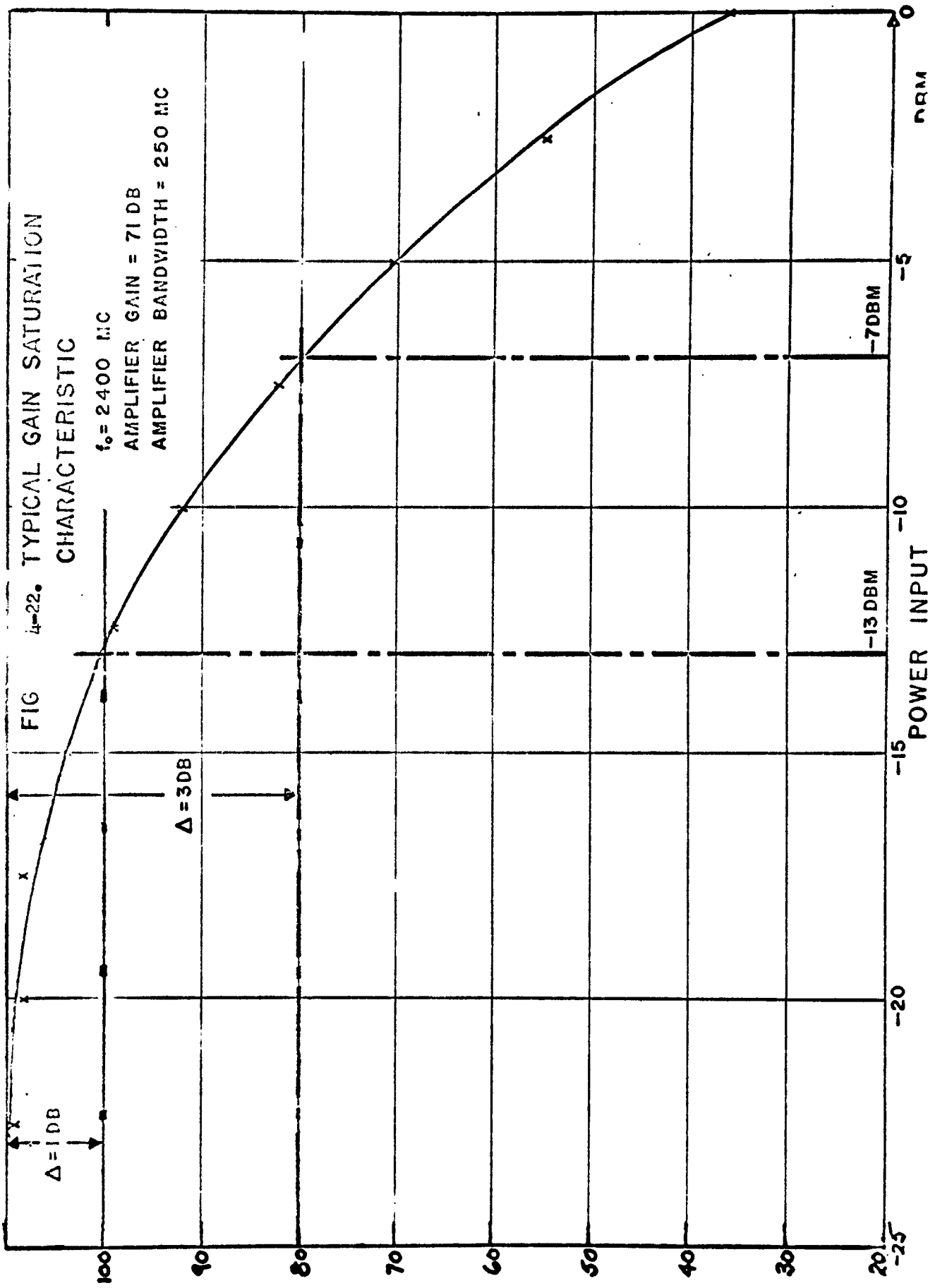
of three 3/32 inch diameter slugs spaced 1.314 inches apart in RG-52/U

waveguide. A response curve for the broadband paramp using this tuner is

shown in Figure 4-23. Different results are obtained, since the frequency

sensitivity of the three slide turners and the triple screw tuner are some-

what different over a broad frequency range.
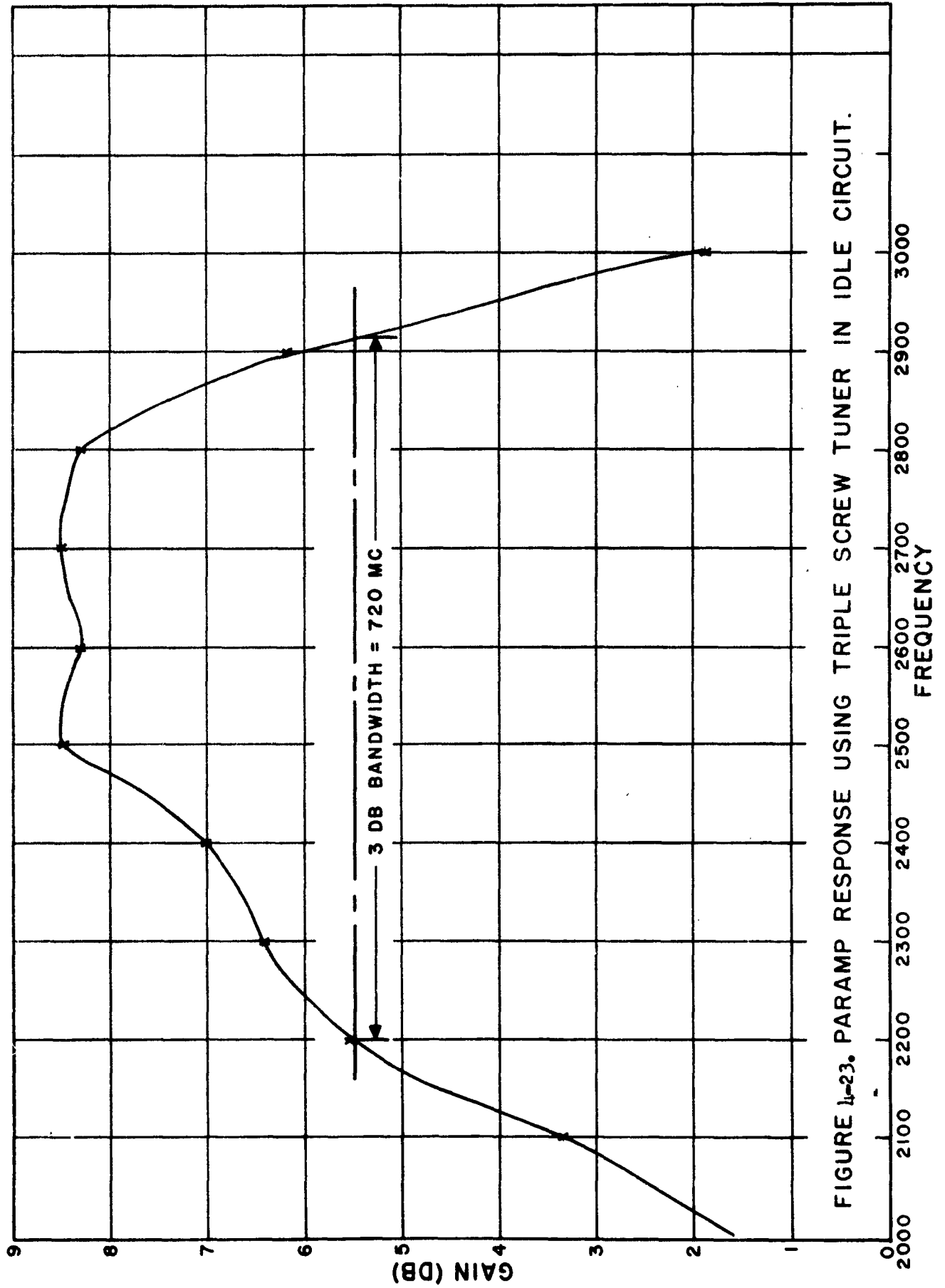
FIGURE 4-23. PARAMP RESPONSE USING TRIPLE SCREW TUNER IN IDLE CIRCUIT.

SECTION 5: CONCLUSIONS

An S-Band, circulator-coupled parametric amplifier can be realized having a gain of 9.5 db, a bandwidth of 830 mc, and a noise figure of approximately 2.1 db. Higher gains can be achieved for narrower bandwidths (e.g. 20-db gain for 330-mc bandwidth). It is significant that this performance has been achieved using a single cartridge type diode without unusually high self-resonant and cutoff frequencies.

External idler loading can be utilized in achieving broadband operation. Although the amplifier noise figure will no longer be optimum, it can be low enough to be quite satisfactory for most applications.

Achieving broadband parametric amplification at microwave frequencies requires integration of the diode parasitic circuit elements (i.e., lead inductance and case capacitance) into broadband signals and idle circuits.

Two simple experimental techniques upon the varactor diodes mounted in a microwave structure can be employed in determining conditions that seem to be necessary for satisfactory broadband parametric amplification at prescribed frequencies.

The signal circuit measurements were made under both static and dynamic conditions (i.e., with and without pump power). The idle-circuit measurements were made under static conditions (i.e., without pump power).

SECTION 6: RECOMMENDED FUTURE WORK

Now that this program has been completed, it seems appropriate to discuss recommended areas of future research and development on broadband parametric amplifiers. This program apparently is but one of three independent efforts within industry that have resulted in significant broadband performance with microwave, semiconductor-diode parametric amplifiers. At Airborne Instruments Laboratory, efforts have been concentrated on the balanced parametric amplifier which employs two pill varactors (8, 9, 10). At Texas Instruments, efforts have been concentrated on a single-diode parametric amplifier using a structure and techniques somewhat different than at RCA (11, 12, 13, 14). The Texas Instruments paramp has only the pump circuit in waveguide, with both the signal and idle circuits in coax. The RCA paramp has both the paramp and idle circuits in waveguide, with only the signal circuit in coax. Performance achieved with the different types of broadband parametric amplifiers is tabulated below.

Company	Center Frequency	Gain	Bandwidth	Noise Figure
RCA	2.5 kmc	9.5 db	830 mc	2.1 db
AIL	5.3 kmc	10 db	500 mc	3.0 db
TI	5.8 kmc	13 db	700 mc	2.4 db
TI	5.8 kmc	13 db	400 mc	2.1 db

Informal discussions with engineering personnel from AIL and TI indicate that other broadband paramps have been developed at L-Band and/or X-Band; however, only published results have been included in the foregoing chart. The AIL amplifier technique utilizes the self-resonant frequency of the diode at the idler frequency. The RCA amplifier technique places the self-resonant frequency of the diode at the signal frequency. The TI amplifier technique uses multi-tuned circuits and apparently does not use the diode self-resonant frequency in such an obvious manner; however, the diode parasitic circuit elements are quite carefully integrated into the signal and idle circuitry. Neither AIL nor TI use external idler loading, while the RCA amplifier does employ such loading.

One area where further theoretical work should be directed is the use of external idler loading. Such loading will undoubtedly prevent realization of optimum noise figure; however, it has not been rigoriously determined as to how much additional bandwidth can be achieved for a given deviation from optimum noise figure.

Another area to be investigated is the performance of broadband paramps when cooled to reduced temperatures. It would be of interest to know how much bandwidth must be sacrificed for a given improvement in noise figure, and to what extent this depends upon the diode semiconductor material.

The problem of increased non-linearity due to anomalous minority-carrier-charge storage effect deserves further attention.

It is somewhat premature to come to any definite conclusions as to the relative merits of the different techniques for broadbanding parametric amplifiers. Both TI and RCA have worked with the AIL balanced paramp with-

out significant success in achieving broadband operation. Nevertheless, it is quite possible that the balanced unit was not given a fair chance. At RCA, good broadband results were obtained extremely late in the program, and work on the balanced paramp had to be abandoned due to the exigencies of the schedule and the fact that a different technique had yielded good broadband results. One question to be answered for all broadband parametric amplifier techniques is, "To what extent does the amplifier performance depend upon the diode parameters, as well as how readily these required tolerances can be realized?"

Another area that should be investigated is phase performance of broadband parametric amplifiers. Possible sources of phase linearity are the ferrite circulator, the signal-line multi-quarter-wave transformer, and the coaxial low-pass filter.

In general, the advanced development of broadband microwave parametric amplifiers has entailed supplementing theoretical methods with a laborious cut-and-try experimental program. Some correlation between theory and experiment has been obtained, although this has not been completely rigorous. The experimental techniques conceived on this program, which provide necessary conditions for broadband paramp operation, are a step in the right direction. Further work of this kind should be of real value, since broadband microwave paramps cannot be scaled, and each amplifier for a new frequency range presents a new developmental problem.

SECTION 7: IDENTIFICATION OF PERSONNEL

Contract DA-39-039-sc-85058 requires an investigative study of the problems entailed in a broadband S-Band reactance amplifier together with the furnishing of experimental reactance amplifiers and manufacturer's drawings thereof and technical reports covering the results of the work accomplished.

Of the total funds allocated for this program at an engineering level, about 29% have been expended during the period October 1, 1961 through March 7, 1962. The program has resulted in a new technique for broadbanding micro-wave parametric amplifiers, and a deliverable model having a bandwidth of 830 mc. This program has been satisfactorily concluded within the allocated funds. A list of key personnel assigned to this contract and the total number of hours spent by each during this period follow:

	Hours Charged to Contract	Hours Worked on Contract
B. Bossard	620	620
R. Pettai	703	703
S. J. Mehlman	---	52
Dr. H. Boyet	---	39
R. M. Kurzrok	31	171
B. Perlman	180	477
E. Markard	654	654

BIBLIOGRAPHY

1. Broadband S-Band Reactance Amplifier, First Quarterly Progress Report, Contract DA 36-039-sc-85058, December 15, 1960.

2. Broadband S-Band Reactance Amplifier, Second Quarterly Progress Report, Contract DA-36-039-sc-85058, March 1, 1961.

3. Broadband S-Band Reactance Amplifier, Third Quarterly Progress Report, Contract DA-36-039-sc-85058, May 1, 1961.

4. Broadband S-Band Reactance Amplifier, Fourth Quarterly Progress Report, Contract DA-36-039-sc-85058, August 1, 1961.

5. Broadband S-Band Reactance Amplifier, Fifth Quarterly Progress Report, Contract DA-36-039-sc-85058, November 1, 1961.

6. B. C. DeLoach, Jr., "Waveguide Parametric Amplifiers", 1961 Solid State Conference Digest, pp. 24-25; February 15, 1961.

7. K. L. Kotzebue, "Optimum Noise Performance of Parametric Amplifiers", Proc. IRE, Vol. 48, pp. 1324-1325, July 1960.

8. Development of Tunable C-Band Reactance Amplifiers, First Quarterly Report, Contract DA-36-039-sc-87405, June 1961.

9. Development of Tunable C-Band Reactance Amplifier, Second Quarterly Report, Contract DA-36-039-sc-87405, September 1961.

10. J. Kliphuis, "C-Band Nondegenerate Parametric Amplifier with 500-mc Bandwidth", Proc. IRE, Vol. 49, p. 961, May 1961.

11. First Quarterly Progress Report on Design and Development of a Low-Noise, Microwave Amplifying Switch, Contract No. 61-0283-d, 2 May 1961.

12. Second Quarterly Progress Report on Design and Development of a Low-Noise, Microwave Amplifying Switch, Contract No. 61-0283-d, 2 Aug.1961.

13.   B. T. Vincent, Jr., "A C-Band Parametric Amplifier with Larbe Band-
width", Proc. IRE, Vol. 49, p. 1682, Nov. 1961.

14.   K. M. Johnson, "Broad-Band S-Band Parametric Amplifier", Proc. IRE,
Vol. 49, p. 1493, December 1961.

APPENDIX I

BASIC THEORY OF VOLTAGE VARIABLE CAPACITANCE

Section 1.1 Derivation of Equivalent Admittance Matrix

We begin by considering a voltage variable capacitor $C = C(v)$ where v is the total voltage across the capacitor (Fig. 1-1a) The total charge Q on the capacitor can also be represented as a function of the impressed voltage (Fig. 1-1b).

$$Q = f(v) \qquad\qquad (1-1)$$

$$(a) \qquad\qquad (b)$$
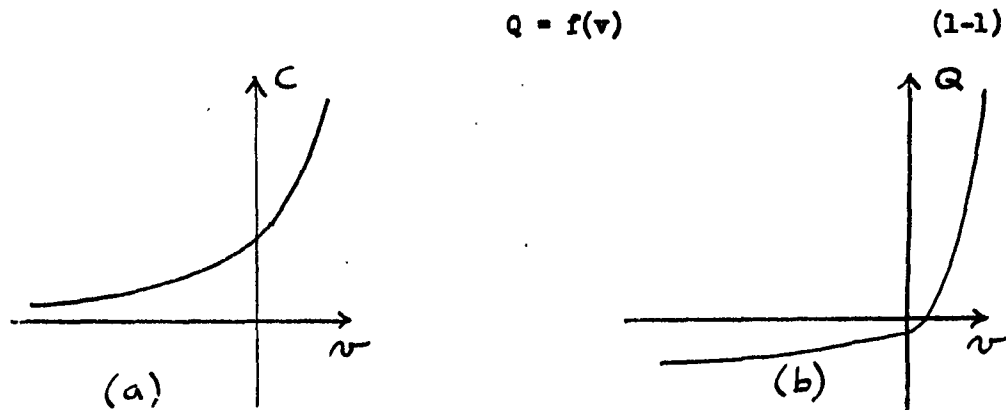
Fig. 1-1. Characteristics of Voltage Variable Capacitance

Using Taylor expansion and taking the first four terms only yields

$$Q = f(v_0) + f'(v_0)(v-v_0) + f''(v_0)\frac{(v-v_0)^2}{2!} + f'''(v_0)\frac{(v-v_0)^3}{3!} \qquad (1-2)$$

The total voltage v will now be taken as the sum of four component voltages: a dc bias voltage v_0, the signal voltage v_1 at a frequency f_1, the idler voltage v_2 at f_2 (also the output voltage in case of a parametric upconverter) and the pump voltage v_3 at f_3, i.e.

$$v = v_0 + v_1 e^{j\omega_1 t} + v_1^* e^{-j\omega_1 t} + v_2 e^{j\omega_2 t} + v_2^* e^{-j\omega_2 t} + v_3 e^{j\omega_3 t} + v_3^* e^{-j\omega_3 t} \qquad (1-3)$$

where by definition

$$v_1 = \frac{|v_1|}{2} e^{j\phi_1}$$

$$v_1^* = \frac{|v_1|}{2} e^{-j\phi_1}$$

$$v_2 = \frac{|v_2|}{2} e^{j\phi_2}$$

$$v_2^* = \frac{|v_2|}{2} e^{-j\phi_2} \qquad (1-4)$$

$$v_3 = \frac{|v_3|}{2} e^{j\phi_3}$$

$$v_3^* = \frac{|v_3|}{2} e^{-j\phi_3}$$

The quantity $|v|$ signifies the physical peak amplitude of the particular voltage. It is seen that the complex conjugate components in Eq. (1-3) combine to give a real, physical voltage across C. For a lower or difference frequency sideband upconverter, the only mode of operation discussed in this paper, the output is taken at the idler frequency f_2, and the three angular frequencies are related as follows

$$\omega_2 = \omega_3 - \omega_1 \qquad (1-5)$$

Since ω_1, ω_2 and ω_3 are in general incommensurate, the phases ϕ_1, ϕ_2 and ϕ_3 could be assumed to be zero. However, for greater generality they will be retained, but the pump phase will be taken as reference and set equal to zero

$$\phi_3 = 0 \qquad (1-6)$$

which means that

$$v_3 = v_3^* = \frac{|v_3|}{2} \qquad (1-7)$$

Substituting Eq. (1-3) into Eq. (1-2) it is evident that the second term $f'(v_0)(v - v_0)$ contains only terms at ω_1, ω_2 and ω_3. In the square term, however, other frequencies appear. If only the three frequencies of interest are retained (the circuits are assumed to be of very low impedance to all others), then in view of Eqs (1-5)

(1-7) the square term of Eq. (1-2) becomes

$$\frac{(v-v_0)^2}{2} = v_2^* v_3 e^{jw_1 t} + v_2 v_3^* e^{-jw_1 t} + v_1^* v_3 e^{jw_2 t} + v_1 v_3^* e^{-jw_2 t} + v_1 v_2 e^{jw_3 t} + v_1^* v_2^* e^{-jw_3 t}$$

(1-8)

Similar treatment of the cubic term shows that among many

terms arising, only the following need be kept:

$$\frac{(v-v_0)^3}{3!} = \left[v_1 e^{jw_1 t} + v_1^* e^{-jw_1 t} \right] \left[\frac{|v_1|^2}{8} + \frac{|v_2|^2}{4} + \frac{|v_3|^2}{4} \right]$$

$$+ \left[v_2 e^{jw_2 t} + v_2^* e^{-jw_2 t} \right] \left[\frac{|v_2|^2}{8} + \frac{|v_3|^2}{4} + \frac{|v_1|^2}{4} \right]$$

$$+ \left[v_3 e^{jw_3 t} + v_3 e^{-jw_3 t} \right] \left[\frac{|v_3|^2}{8} + \frac{|v_1|^2}{4} + \frac{|v_2|^2}{4} \right]$$ (1-9)

Since the idler and signal amplitudes are assumed to be much

smaller than that of the pump, Eq. (1-9) simplifies to -

$$\frac{(v-v_0)^3}{3!} = \left\{ v_1 e^{jw_1 t} + v_1^* e^{-jw_1 t} \right\} \frac{|v_3|^2}{4} + \left\{ v_2 e^{jw_2 t} + v_2^* e^{-jw_2 t} \right\} \frac{|v_3|^2}{4}$$

$$+ \left\{ v_3 e^{jw_3 t} + v_3 e^{-jw_3 t} \right\} \frac{|v_3|^2}{8}$$ (1-10)

Let us also write the total charge Q as

$$Q = q_0 + q_1 e^{jw_1 t} + q_1^* e^{-jw_1 t} + q_2 e^{jw_2 t} + q_2^* e^{-jw_2 t} + q_3 e^{jw_3 t} + q_3 e^{-jw_3 t}$$ (1-11)

If Eqs. (1-8), (1-10) and (1-11) are now substituted in Eq. (1-2)

and terms of like frequency are grouped together, then

$$q_0 = f(v_0)$$

$$q_1 e^{jw_1 t} = \left[\left(f'(v_0) + f'''(v_0) \frac{|v_3|^2}{4} \right) v_1 + f''(v_0) v_2^* v_3 \right] e^{jw_1 t}$$

$$q_1^* e^{-jw_1 t} = \left[\left(f'(v_0) + f'''(v_0) \frac{|v_3|^2}{4} \right) v_1^* + f''(v_0) v_2 v_3^* \right] e^{-jw_1 t}$$ (1-12)

$$q_2 e^{jw_2 t} = \left[\left(f'(v_0) + f'''(v_0) \frac{|v_3|^2}{4} \right) v_2 + f''(v_0) v_1^* v_3 \right] e^{jw_2 t}$$

$$q_2^* e^{-i\omega_2 t} = \left[\left(f'(v_0) + f'''(v_0) \frac{|v_3|^2}{4}\right) v_2^* + f''(v_0) v_1^* v_3 \right] e^{-i\omega_2 t}$$

$$q_3 e^{i\omega_3 t} = \left[\left(f'(v_0) + f'''(v_0) \frac{|v_3|^2}{8}\right) v_3 + f''(v_0) v_1 v_2 \right] e^{i\omega_3 t} \quad \text{(1-12 con't)}$$

$$q_3^* e^{-i\omega_3 t} = \left[\left(f'(v_0) + f'''(v_0) \frac{|v_3|^2}{8}\right) v_3 + f''(v_0) v_1^* v_2^* \right] e^{-i\omega_3 t}$$

It is of particular interest to examine the following pair of equations*

$$q_1 e^{i\omega_1 t} = \left[\left(f'(v_0) + f'''(v_0) \frac{|v_3|^2}{4}\right) v_1 + \left(f''(v_0) v_3\right) v_2^* \right] e^{i\omega_1 t} \quad \text{(1-13)}$$

$$q_2^* e^{-i\omega_2 t} = \left[\left(f''(v_0) v_3\right) v_1 + \left(f'(v_0) + f'''(v_0) \frac{|v_3|^2}{4}\right) v_2^* \right] e^{-i\omega_2 t} \quad \text{(1-14)}$$

The above equations resemble those of a four-terminal or two-port network. In this case, however, the two ports correspond to different frequency domains, ω_1 and ω_2. The significance of Eqs. (1-13) and (1-14) becomes more apparent when both are differentiated with respect to time.

After differentiating and dropping the time dependence we obtain:

$$\frac{dq_1}{dt} = I_1 = i\omega_1 \left[f'(v_0) + f'''(v_0) \frac{|v_3|^2}{4} \right] v_1 + i\omega_1 \left[f''(v_0) v_3 \right] v_2^* \quad \text{(1-15)}$$

$$\frac{dq_2}{dt} = I_2^* = -i\omega_2 \left[f''(v_0) v_3 \right] v_1 - i\omega_2 \left[f'(v_0) + f'''(v_0) \frac{|v_3|^2}{4} \right] v_2^* \quad \text{(1-16)}$$

* This is arbitrary; the other pair involving q_1^* and q_2 could have been taken as well.

These equations are in the familiar form of admittance description of a general four-terminal network.

Eqs. (1-15) and (1-16) show clearly that there is coupling between v_1 and v_2^* through the action of the pump voltage. The presence of the pump therefore couples the signal voltage at f_1 to the conjugate of the idler voltage at f_2. It is to be noted that the quantities corresponding to y_{12} and y_{21} are of opposite sign, which means that the input admittance can be negative. This is easily seen if one considers the coupling of v_1 to I_2^* and back to I_1 again via v_2^*. The total phase shift is zero since a shift to $+j$ is experienced in going from v_1 to I_2^* and $-j$ is continuing from v_2^* to I_1. In passive linear circuits the signs of y_{12} and y_{21} are equal and a total phase shift of 180° would be obtained.

Eqs. (1-12) show that four more coupled pairs exist, one for example being between v_1 and v_3^* but there the coupling occurs either via v_1 or v_2, being much weaker on account of v_1 and $v_2 \ll v_3$. As a result, those couplings are of no particular interest in the present case and will not be considered further.

Returning to Eqs. (1-15) and (1-16) we note that $f'(v) = \dfrac{dQ}{dv}$ $= C$ and therefore $f'(v_0) = C_0$, the operating point. Since $f'''(v_0)$ is dimensionally also a capacitance we let

$$C_0 + f''' \frac{|v_3|^2}{4} = C_T \qquad (1\text{-}17)$$

The physical significance of C_T can be seen from Fig. 1.2. With no pump voltage applied $C_T = C_0$, which is the quiescent point determined by the applied dc bias v_0. With v_3 applied, the curvature of the non-linear capacitance causes the effective operating point to shift slightly from C_0 to C_T. This is analogous to the appearance of

a dc term in devices having non-linear transfer characteristics such as a square law detector.

The term $f''(v_o)v_3$ can also be given a physical meaning. From Eq. (1-7) we note that v_3 is a real quantity, equal to $\frac{|v_3|}{2}$. Hence

$$f''(v_o)v_3 = \frac{|v_3|}{2} f''(v_b) \qquad (1\text{-}18)$$

and it thus represents the line segment shown in Fig. 1-2 below
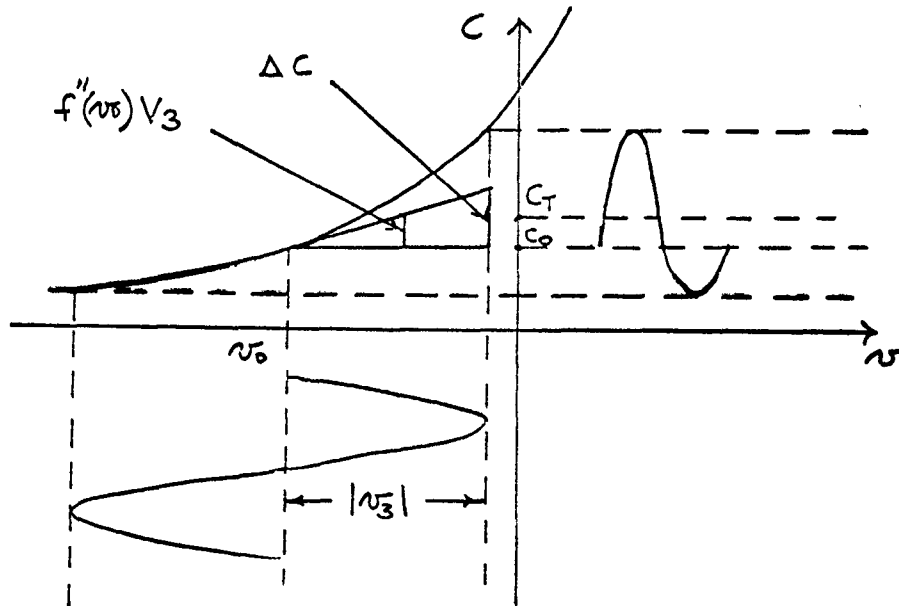
Fig. 1-2. Relationship between C_o, C_T and $\triangle C$

For brevity let

$$v_3 f''(v_o) = \frac{\triangle C}{2} \qquad (1\text{-}19)$$

We can now rewrite Eqs. (1-15) and (1-16)

$$I_1 = j\omega_1 C_T v_1 + j\omega_1\left(\frac{\triangle C}{2}\right)v_2^* \qquad (1\text{-}20)$$

$$I_2^* = -j\omega_2\left(\frac{\triangle C}{2}\right)v_1 - j\omega_2 C_T v_2^* \qquad (1\text{-}21)$$

or in matrix form

$$\left\|\begin{array}{c} I_1 \\ I_2^* \end{array}\right\| = \left\|y\right\| \times \left\|\begin{array}{c} v_1 \\ v_2^* \end{array}\right\| \qquad (1\text{-}22)$$

where

$$\|y\| = \begin{Vmatrix} y_{11} & y_{12} \\ y_{21} & y_{22} \end{Vmatrix} = \begin{Vmatrix} j\omega_1 C_T & j\omega_1\left(\frac{\Delta C}{2}\right) \\ -j\omega_2\left(\frac{\Delta C}{2}\right) & -j\omega_2 C_T \end{Vmatrix} \qquad (1\text{-}23)$$

Section 1.2 Equivalent Circuits for Ideal Varactors*

The relationships (1-20) and (1-21), and their matrix (1-23)
can readily be represented by an equivalent circuit which contains
two passive elements and two voltage-controlled current sources.
Fig. 1-3 shows the resulting network.
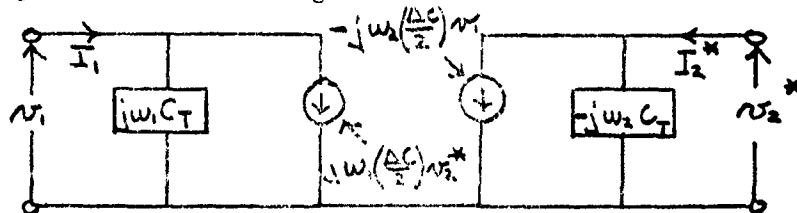
Fig. 1-3. Current Source Representation of Non-linear
Capacitance

Henceforth y_{11} and y_{22} will be called the self-admittances of
the signal and idler frequencies respectively, whereas $y_{12} v_2^*$ and $y_{21} v_1$ are
the coupling terms in the form of voltage-controlled current sources.

This representation is, of course, not the only one possible. For
example, the matrix (1-23) could be easily inverted and the resulting
Z-matrix would then yield the network shown in Fig. 1-4 on the following
page.

----

* Henceforth the terms "Varactor", "diode" and "non-linear capacitance"
will be used interchangeably, all referring to the variable capacitance
semiconductor juncition diode.
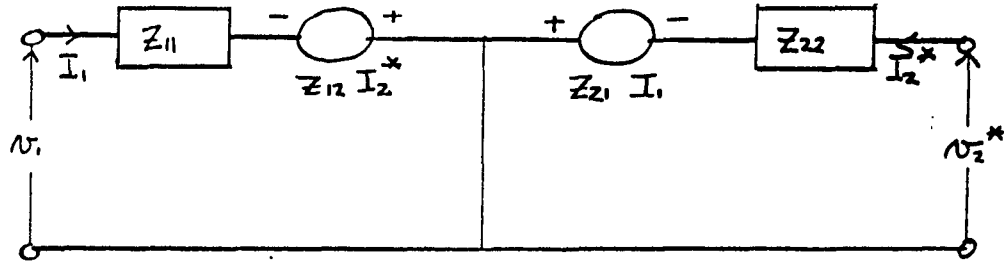
Fig. 1-4. Voltage Source Representation of Non-linear
Capacitance

Here

$$z_{11} = \frac{y_{22}}{det} = -j\frac{1}{\omega_1 C_T K^2}$$

$$z_{12} = -\frac{y_{12}}{det} = -j\frac{1}{\omega_2 C_T^2 K^2}\left(\frac{\Delta C}{2}\right)$$

$$z_{21} = -\frac{y_{21}}{det} = j\frac{1}{\omega_1 C_T^2 K^2}\left(\frac{\Delta C}{2}\right)$$

$$z_{22} = \frac{y_{11}}{det} = j\frac{1}{\omega_2 C_T K^2} \quad ,$$

(1-24)

and for convenience

$$k^2 \equiv 1 - \left(\frac{\Delta C}{2 C_T}\right)^2 .$$

(1-25)

While from a theoretical standpoint the two representations, i.e.
either contr lled voltage or controlled current sources, are completely
equivalent, only the latter type will be used in the analyses. The
reason for this choice lies in the greater usefulness that the shunt
representation has in most waveguide network elements (tuners, irises etc.)
are shunt devices by nature. Furthermore, the variable capacitor itself,
in form of a Varactor diode, is usually shunted across the waveguide in
most physical parametric devices. The representation of Fig. 1-3 is
therefore more natural and can be more easily combined with the rese of
the circuit to simplify the analysis.

Section 2.1 Modified Admittance Matrix

In the foregoing analysis the Varactor diode was assumed to be a pure variable capacitance. This is a very much idealized picture since a conventional, physical diode is known to contain a number of parasitic elements such as case capacitance, lead inductance and ohmic resistance. A more accurate equivalent circuit for these diodes therefore is shown in Fig. 1-5.
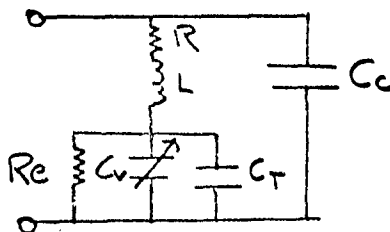
Fig. 1-5. Equivalent Circuit of Varactor Diode

In the figure R is the spreading resistance which includes the spreading effect of the p-n junction as well as the ohmic contact losses. L and C_c are respectively the lead inductance and case capacitance associated with the diode package. R_e is the leakage resistance. The voltage-variable capacitance C has been shown separated into C_T and C_v in order to emphasize that the variations of capacitance are superimposed on a given quiescent value of C, namely C_T.

Typical values for commercially available variable capacitance diodes are presented in Table 2-1 below.

$C_T = 0.5 - 4$ μμf

$R = 1 - 10$ ohms

$L = 0.5 - 5$ mμh

$C_c = 0.1 - 0.3$ μμf

$R_e = 1$ megohm

Table 2-1. Parameters of Actual Varactors

In most diodes the case capacitance C_c is small enough to be neglected. Similarly at frequencies above VHF the leakage resistance R_e in parallel with C_T can be ignored if there is no pump voltage excursion into the forward conduction region. In view of this the equivalent circuit of the diode will be taken as that shown in Fig. 1-6.
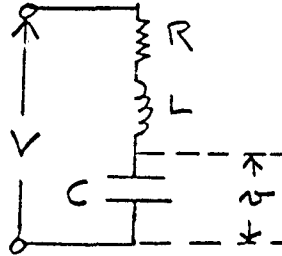
Fig. 1-6. Simplified Equivalent Circuit of Varactor Diode

In previous analysis (Chapter I) an admittance matrix was derived for the variable capacitance only, i.e.

$$\left\| \begin{array}{c} I_1 \\ I_2^* \end{array} \right\| = \left\| y \right\| \times \left\| \begin{array}{c} V_1 \\ V_2^* \end{array} \right\|$$

In order to obtain an admittance matrix in terms of voltages across the total network, we first let V be the voltage across the external, physical terminals of the diode. We shall then seek a transfer matrix such that

$$\left\| \begin{array}{c} V_1 \\ V_2^* \end{array} \right\| = \left\| \begin{array}{cc} T_{11} & T_{12} \\ T_{21} & T_{22} \end{array} \right\| \times \left\| \begin{array}{c} V_1 \\ V_2^* \end{array} \right\|. \tag{2-2}$$

If we let

$$R + j\omega_1 L = Z_1$$

and

$$R + j\omega_1 L = Z_2 \tag{2-3}$$

then from Fig. 1-6 and using Eq. (2-1)

$$v_1 = V_1 - I_1 Z_1 = V_1 - (y_{11}v_1 + y_{12} v_2^*) Z_1$$

$$v_2^* = V_2^* - I_2^* Z_2^* = V_2^* - (y_{21}v_1 + y_{22}v_2^*) Z_2^* \qquad (2\text{-}4)$$

Eqs. (2-4) yield

$$v_1 = \frac{V_1 - y_{12} Z_1 v_2^*}{(1 + y_{11} Z_1)}$$

$$v_2^* = \frac{V_2^* - y_{21} Z_2^* v_1}{(1 + y_{22} Z_2^*)} \qquad (2\text{-}5)$$

and from these finally

$$v_1 = V_1 \left[\frac{1 + y_{22} Z_2^*}{D} \right] + V_2^* \left[-\frac{y_{12} Z_1}{D} \right] \qquad (2\text{-}6)$$

$$v_2^* = V_1 \left[-\frac{y_{12} Z_2^*}{D} \right] + V_2^* \left[\frac{1 + y_{11} Z_1}{D} \right] \qquad (2\text{-}7)$$

where

$$D = 1 + y_{11} Z_1 + y_{22} Z_2^* + Z_1 Z_2^* \triangle \qquad (2\text{-}8)$$

and $\triangle$ is the determinant of matrix (1-23).

A comparison of Eqs. (2-2), (2-6) and (2-7) gives the desired elements of the transfer matrix

$$\left\| \begin{matrix} T_{11} & T_{12} \\ T_{21} & T_{22} \end{matrix} \right\| = \frac{1}{D} = \left\| \begin{matrix} (1 + y_{22} Z_2^*) & (-y_{12} Z_1) \\ (-y_{21} Z_2^*) & (1 + y_{11} Z_1) \end{matrix} \right\| \qquad (2\text{-}9)$$

We now have from Eqs. (2-1) and (2-2)

$$\left\| \begin{matrix} I_1 \\ I_2^* \end{matrix} \right\| = \left\| \begin{matrix} (y_{11} T_{11} + y_{12} T_{21}) & (y_{11} T_{12} + y_{12} T_{22}) \\ (y_{21} T_{11} + y_{22} T_{21}) & (y_{21} T_{12} + y_{22} T_{22}) \end{matrix} \right\| \times \left\| \begin{matrix} v_1 \\ v_2^* \end{matrix} \right\| \qquad (2\text{-}10)$$

and a substitution for the T's yields

$$\left\| \begin{matrix} I_1 \\ I_2^* \end{matrix} \right\| = \frac{1}{D} \left\| \begin{matrix} (y_{11} + Z_2^* \triangle) & y_{12} \\ y_{21} & (y_{22} + Z_1 \triangle) \end{matrix} \right\| \times \left\| \begin{matrix} v_1 \\ v_2^* \end{matrix} \right\| \qquad (2\text{-}11)$$

Hence the new admittance matrix, referred to the physical terminals of a diode, can be written as

$$\|Y\| = \frac{1}{D} \left\| \begin{array}{cc} (y_{11} + z_2^* \Delta) & y_{12} \\ y_{21} & (y_{22} + z_1 \Delta) \end{array} \right\| \qquad (2\text{-}12)$$

In order to evaluate individual terms of Eq. (2-12), use will be made of Eqs. (1-23), (2-3) and 2-8. Thus by direct substitution

$$D = 1 + y_{11} z_1 + y_{22} z_2^* + z_1 z_2^* \Delta$$

$$= 1 + j w_1 C_T (R + j w_1 L) + (-j w_2 C_T)(R - j w_2 L) +$$

$$(R + j w_1 L)(R - j w_2 L) \Delta$$

where

$$\Delta = y_{11} y_{22} - y_{12} y_{21} = w_1 w_2 \left\{ C_T^2 - \left(\frac{\Delta C}{2}\right)^2 \right\} = w_1 w_2 C_T^2 k^2$$

by virtue of Eq. (1-25). Hence

$$D = 1 - w_1^2 L C_T + j w_1 RC - w_2^2 L C_T - j w_2 RC_T + \qquad (2\text{-}13)$$
$$\left[R^2 C_T^2 + w_1 w_2 L^2 C_T^2 + j w_1 L RC_T^2 - j w_2 L RC_T^2 \right] k^2 w_1 w_2$$

At this point let us introduce two new quantities, the series resonant frequenxy w_o and the cutoff frequency w_c. By definition

$$w_o^2 = \frac{1}{L C_T} \qquad (2\text{-}14)$$

$$w_c = \frac{1}{R C_T} \qquad (2\text{-}15)$$

Furthermore, let

$$\frac{w_1}{w_o} = \beta_1 \qquad \frac{w_1}{w_c} = \varepsilon_1 \qquad (2\text{-}16)$$

$$\frac{w_2}{w_o} = \beta_2 \qquad \frac{w_2}{w_c} = \varepsilon_2 \qquad (2\text{-}17)$$

Eq. (2-13) can now be written in a simpler form, from which the physical nature of D can be more readily ascertained.

$$D = 1 - \beta_1^2 - \beta_2^2 + k^2(\beta_1 \beta_2 + \epsilon_1 \epsilon_2) + j\left[\epsilon_1 - \epsilon_2 + k^2 \epsilon_1 \beta_2(\beta_1 - \beta_2)\right] \quad (2\text{-}18)$$

Similar substitutions result in

$$y_{11} + z_2^* \Delta = j\omega_1 C_T\left\{1 - k^2(\beta_2^2 + j\epsilon_2)\right\} \quad (2\text{-}19)$$

and

$$y_{22} + z_1 \Delta = -j\omega_2 C_T\left\{1 - k^2(\beta_1^2 - j\epsilon_1)\right\} \quad (2\text{-}20)$$

Eq. (2-12) can now be written in its final form as

$$\|y\| = \left\|\begin{matrix} y_{11} & y_{12} \\ y_{21} & y_{22} \end{matrix}\right\| = \frac{1}{D} \left\|\begin{matrix} j\omega_1 C_T\left\{1 - k^2(\beta_2^2 + j\epsilon_2)\right\} & j\omega_1\left(\frac{\Delta c}{2}\right) \\ -j\omega_2\left(\frac{\Delta c}{2}\right) & -j\omega_2^* C_T\left\{1 - k^2(\beta_1^2 - j\epsilon_1)\right\} \end{matrix}\right\| \quad (2\text{-}21)$$

As a check, it should be noted that if the parasitic resistance R and the lead inductance L are made very small, then ω_1 and ω_2 become large, the quantities β_1, β_2, ϵ_1 and ϵ_2 tend toward zero and D will approach unity. In the limit the matrix (2-21) will become identically equal to that of (1-23) which, it will be recalled, described the behavior of an idealized non-linear capacitance .

It should be stated that in this as well as in forthcoming analysis the pump voltage v_3 across the p-n junction capacitance (and hence ΔC) is assumed independent of ω_0 and ω_0. Obviously ω_0 and ω_0 do affect the voltage drop across C_T, but a simplifying assumption is made that regardless of ω_0 or ω_0 the pump power is adjusted to yield the same pump voltage swing across the junction capacitance.

Section 2.2   Modified Impedance Matrix

Although the equivalent impedance description of a voltage variable capacitor, as first presented in Section 1.2, will not be used in the analysis of the parametric upconverter, the modified impedance matrix is derived for the sake of completeness.

Since the series arrangement of parasitic elements in Fig. 1-6 already suggests an impedance description, the derivation becomes almost trivial. Starting with the four-terminal model of the diode as shown in Fig. 1-4 and its impedance matrix, Fig. 1-6 gives

$$V_1 = V_1 - I_1 Z_1 = z_{11} I_1 + z_{12} I_2^*$$

$$v_2^* = V_2^* - I_2^* z_2^* = z_{21} I_1 + z_{22} I_2^*$$

From these

$$V_1 = (z_{11} + Z_1) + z_{12} I_2^*$$

$$V_2^* = z_{21} I_1 + (z_{22} + z_2^*) I_2^*$$

Substitutions from Eqs. (1-24) and (2-3) finally lead to

$$\|z\| = \left\| \begin{array}{cc} R + j(\omega_1 L - \frac{1}{\omega_1 C_T K^2}) & -j \frac{\frac{\Delta C}{2}}{\omega_2 C_T^2 K^2} \\ j \frac{\frac{\Delta C}{2}}{\omega_1 C_T^2 K^2} & \left\{ R - j(\omega_2 L - \frac{1}{\omega_2 C_T K^2}) \right\} \end{array} \right\| \qquad (2\text{-}22)$$

Section 2.3 Resonance Factor

The most important modification of the original admittance matrix (1-23) is the appearance of D which will henceforth be referred to as the resonance factor. In the following sections its effect on the performance of the parametric upconverter will be discussed in detail. Here we shall make a study of the quantitative behavior of the resonance factor as a function of the frequencies involved.

To repeat

$$D = 1 - \beta_1^2 - \beta_2^2 + K^2 (\beta_1^2 \beta_2^2 + \xi_1 \xi_2) + j \left[\xi_1 - \xi_2 + K^2 \xi_1 \beta_2 (\beta_1 - \beta_2) \right]$$

In general D will be a complex number, involving both the series resonant frequency ω_0 and the cutoff frequency ω_c. While the complex D could be analyzed, rather complicated and uninformative expressions

would result. Fortunately the state of the art of making variable
capacitance diodes has been brought to a stage where diodes with very
high cutoff frequencies ($>$ 100 kmc) are becoming available. Since, on
the other hand, the operating frequencies ω_1 and ω_2 are in low microwave
regions, the quantities

$$\varepsilon_1 = \frac{\omega_1}{\omega_c} \qquad \qquad \varepsilon_2 = \frac{\omega_2}{\omega_c}$$

can be neglected, and thus the resonance factor becomes a real number.
The series resonant frequency ω_0 is, however, very much lower than ω_c.
For present day diodes ω_0 rarely reaches 10 kmc. Most commercially
available units exhibit series resonance at frequencies as low as 2500 mc.
These frequencies lie well within the operating range.

Subject to the assumption of very high ω_c the resonance factor is
given by

$$D = 1 - \beta_1^2 - \beta_2^2 + \kappa^2 \beta_1^2 \beta_2^2 \qquad (2\text{-}23)$$

where

$$\beta_1 = \frac{\omega_1}{\omega_0} \qquad \beta_2 = \frac{\omega_2}{\omega_0} \qquad \kappa^2 = 1 - \left(\frac{\Delta c}{2 c_T}\right)^2.$$

APPENDIX II

DERIVATION OF GENERAL PARAMETRIC UPCONVERTER

The pumped varactor diode can be represented by the following admittance matrix (also see First Quarterly Progress Report, Signal Corps Contract DA-36-039-sc-85058, DA Project No. 3A99-21-001-01 pp 4-5, 35-49).

$$|Y| = \begin{vmatrix} \dfrac{j\omega_1 C_0}{\left[1 - \left(\dfrac{\omega_1}{\omega_0}\right)^2\right]} & \dfrac{j\omega_1 \left(\dfrac{\Delta C}{2}\right)}{D} \\ -\dfrac{j\omega_2 \left(\dfrac{\Delta C}{2}\right)}{D} & -\dfrac{j\omega_2 C_0}{\left[1 - \left(\dfrac{\omega_2}{\omega_0}\right)^2\right]} \end{vmatrix} \qquad (2\text{-}1)$$

where

$$D \doteq \left[1 - \left(\frac{\omega_1}{\omega_0}\right)^2\right]\left[1 - \left(\frac{\omega_2}{\omega_0}\right)^2\right] \qquad (2\text{-}2)$$

ω_1 = signal (input) frequency

ω_2 = idler (output) frequency

ω_0 = series resonant frequency of the diode.

The cutoff frequency of the diode is assumed such that

$$\omega_c \gg \omega_0$$

The complete circuit of the upconverter can now be drawn as follows:
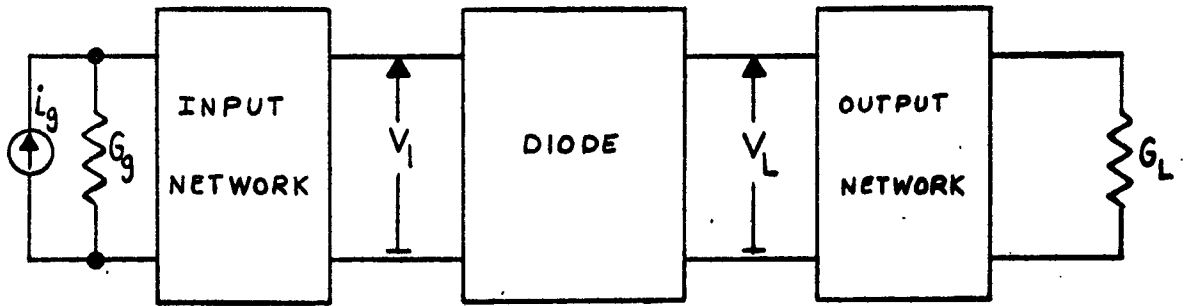
Figure 2-1   Basic Structure of the Upconverter

The self-susceptances Y_{11} and Y_{22} will now be combined with the respective networks. Furthermore, applying Norton's Theorem to the input side, we finally obtain the circuit below
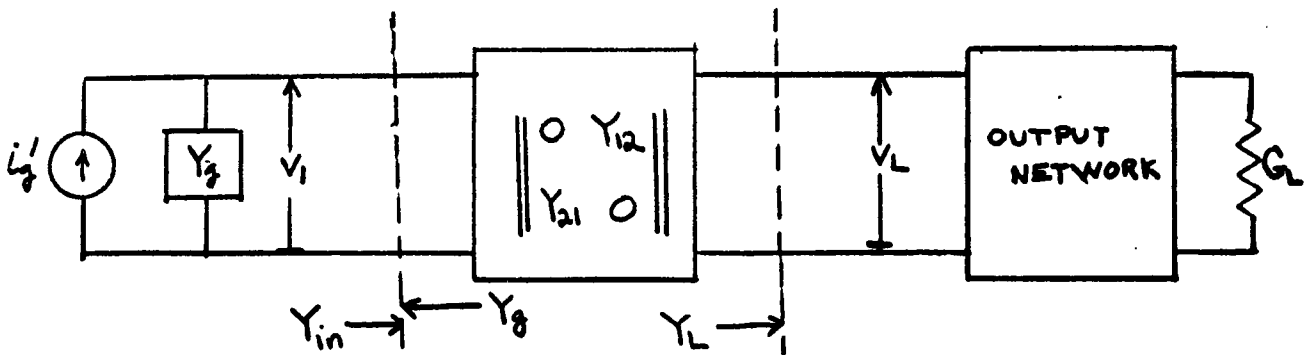
Figure 2-2   Upconverter Circuit After Reduction

Power across G_L is given by

$$P_L = \left|\frac{V_L}{V_1}\right|^2 \left|V_1\right|^2 R_e\,(Y_L) \qquad\qquad (2\text{-}3)$$

Maximum available power from the input generator is

$$P_o = \frac{\left|i_g'\right|^2}{4 \, R_e \, (Y_g)} = \frac{\left|V_1\right|^2 \left|Y_g + Y_{in}\right|^2}{4 \, R_e \, (Y_g)} \qquad (2\text{-}4)$$

Hence the over-all transducer gain is

$$G_T = \frac{P_L}{P_o} = \left|\frac{V_L}{V_1}\right|^2 \frac{4 \, R_e \, (Y_g) \, R_e \, (Y_L)}{\left|Y_g + Y_{in}\right|^2} \qquad (2\text{-}5)$$

The individual terms can be easily obtained by applying the equations for voltage gain and input admittance of conventional four-terminal networks. Thus

$$\left|\frac{V_L}{V_1}\right|^2 = \left|\frac{Y_{21}}{Y_{22} + Y_L{}^*}\right|^2 = \left|\frac{Y_{21}}{Y_L}\right| \qquad (2\text{-}6)$$

where it will be remembered that Y_{11} and Y_{22} were lumped with the respective networks. Hence shown in Figure 2-2 the diagonal terms of the matrix (2-1) are zero.

In a similar manner

$$\left|Y_g + Y_{in}\right|^2 = \left|Y_g - \frac{Y_{12} \, Y_{21}}{Y_L{}^*}\right|^2 = \frac{\left|Y_g \, Y_L - Y_{12} \, Y_{21}\right|^2}{\left|Y_L{}^*\right|^2} \qquad (2\text{-}7)$$

The reason for the complex conjugate of Y_L follows from the initial derivation of the admittance matrix of the diode. It will be remembered that the pump coupled the signal voltage at f_1 to the conjugate of the idler voltage at f_2. As a result, all admittances in the idler circuit, as far as the analysis is concerned, are ratios of a conjugate current I_2 to a conjugate

voltage V_2, and must therefore be entered in equations as such. As an illustration, the diode self-susceptance Y_{22} is physically a capacitive susceptance below the series resonance. In the matrix (2-1) however, it appears with a minus sign.

Combining Equations (2-6), (2-7), and (2-5) yields

$$G_T = \frac{4 \left| Y_{21} \right|^2 R_e (Y_g) R_e (Y_L)}{\left| Y_g Y_L^* - Y_{12} Y_{21} \right|^2} \qquad (2-8)$$

If Y_{12} and Y_{21} in Equation (2-8) are replaced by their equivalents from the matrix (2-1), one obtains the transducer gain equation for a parametric upconverter.

$$G_T = \frac{4 \left(\omega_2 \frac{\Delta c}{2} \right)^2 R_e (Y_g) R_e (Y_L)}{D^2 \left[\left| Y_g Y_L^* - \frac{\omega_1 \omega_2 \left(\frac{\Delta c}{2} \right)^2}{D^2} \right| \right]^2} \qquad (2-9)$$

APPENDIX III

GAIN DERIVATION OF A CIRCULATOR COUPLED PARAMETRIC AMPLIFIER

(Reflection Type)

The scattering matrix of the three port circulator shown in Figure 3-1

$$S = \begin{Vmatrix} 0 & 0 & 1 \\ 1 & 0 & 0 \\ 0 & 1 & 0 \end{Vmatrix} \tag{3-1}$$
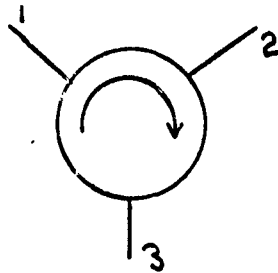
Figure 3-1   Three Port Circulator

From this the normalized Y-matrix becomes

$$Y' = \begin{Vmatrix} 0 & 1 & -1 \\ -1 & 0 & 1 \\ 1 & -1 & 0 \end{Vmatrix} \tag{3-2}$$

Unnormalizing the Y-matrix

$$Y = \begin{Vmatrix} 0 & G_o & -G_o \\ -G_o & 0 & G_o \\ G_o & -G_o & 0 \end{Vmatrix} \tag{3-3}$$

Now let port 2 of the circulator be terminated by a paramp with an input admittance Y_{in}.

Then

$$I_2 = - V_2 Y_{in} \tag{3-4}$$

From Equations (3-3) and (3-4)

$$-V_2 Y_{in} = - V_1 G_o + V_3 G_o \tag{3-5}$$

or

$$V_2 = V_1 \frac{G_o}{Y_{in}} - V_3 \frac{G_o}{Y_{in}} \tag{3-6}$$

and

$$I_1 = \frac{G_o}{Y_{in}} \left[G_o V_1 - G_o V_3 \right] - G_o V_3$$

or

$$I_1 = \frac{G^2_o}{Y_{in}} V_1 - \left[\frac{G^2_o}{Y_{in}} + G_o \right] V_3 \tag{3-7}$$

Similarly

$$I_3 = G_o \left[1 - \frac{G_o}{Y_{in}} \quad V_1 + \frac{G^2_o}{Y_{in}} \right] V_3 \tag{3-8}$$

Thus the Y-matrix for a circulator paramp combination becomes

$$\|Y\| = \left\| \begin{array}{cc} \dfrac{G^2_{o}}{Y_{in}} & -G_{o}\left[\dfrac{G_{o}}{Y_{in}} + 1\right] \\ \\ G_{o}\left[1 - \dfrac{G_{o}}{Y_{in}}\right] & \dfrac{G^2_{o}}{Y_{in}} \end{array} \right\| \qquad (3\text{-}9)$$

Since the numbering scheme of the ports is immaterial we change for convenience to the 1-2 notation. The circuit could then be drawn as indicated below
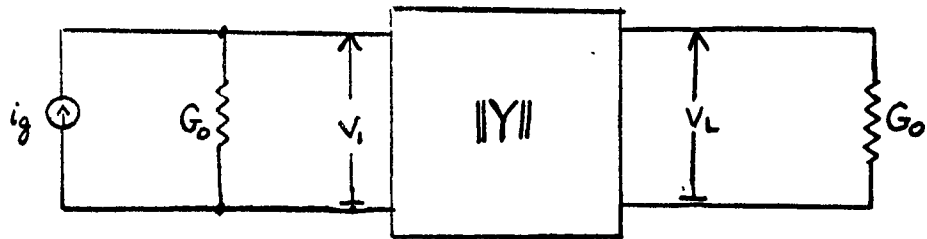
Figure 3-2   Circulator Paramp Equivalent Circuit

From Figure 3-2

$$P_o = \frac{|i_g|^2}{4\,G_o} \quad \text{and} \quad P_L = |V_L|^2\,G_o = \left|\frac{V_L}{V_1}\right|^2 |V_1|^2\,G_o \qquad (3\text{-}10)$$

$$\frac{P_L}{P_o} = \left|\frac{V_L}{V_1}\right|^2$$

since P_o can be written as

$$P_o = \frac{|V_1|^2 |G_o + G_{in}|^2}{4\,G_o}$$

and

$$G_{in} = G_o \; .$$

From network theory and Equation (3-9)

$$\left|\frac{V_L}{V_1}\right|^2 = \left|\frac{Y_{21}}{Y_{22} + Y_L}\right|^2 = \left|\frac{1 - \dfrac{G_o}{Y_{in}}}{1 + \dfrac{G_o}{Y_{in}}}\right|^2 \tag{3-11}$$

With no additional networks in the input or output the paramp can be represented as
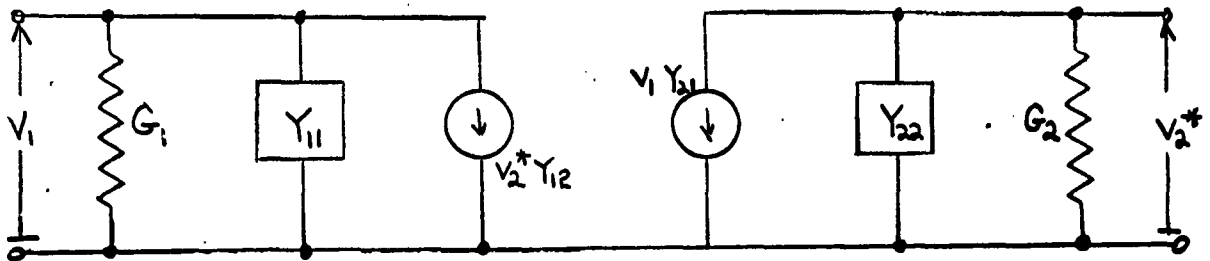
Figure 3-3 Equivalent Circuit of Parametric Amplifier

where G_1 and G_2 are the circuit losses present.

Y_{in} is obtained from Figure 3-3 and becomes

$$Y_{in} = (G_1 + Y_{11}) - \frac{\omega_1\,\omega_2 \left(\dfrac{\Delta C}{2}\right)^2}{D^2 \left[G_2 + Y_{22}\right]}$$

The admittance terms Y_{11}, Y_{12}, and Y_{22} used just above and in Figure 3-3 refer to the parametric diode admittance matrix.

From Equation (3-11)

$$G_T = \frac{P_L}{P_0} = \frac{\left| Y_{in} - G_0 \right|^2}{\left| Y_{in} + G_0 \right|^2}$$

and

$$G_T = \left| \frac{(G_1 + Y_{11} - G_0) - \dfrac{\omega_1 \omega_2 \left(\dfrac{\Delta c}{2}\right)^2}{D^2 \left[Y_2 + Y_{22}\right]}}{(G_1 + Y_{11} + G_0) - \dfrac{\omega_1 \omega_2 \dfrac{\Delta c^2}{2}}{D^2 \left[Y_2 + Y_{22}\right]}} \right| \qquad (3\text{-}12)$$

where G_2 has been changed to Y_2 since in a general case the idler may be terminated in a complex network instead of just G_2.

In general the negative conductance term in the circulator gain equation is not large enough to overcome the positive conductance of the device. Therefore it is sometimes necessary to place a transformer in port 2 of the circulator. The input admittance of the parametric amplifier then becomes $N^2 Y_{in}$ where N is the turns ratio of the transformer. Similarly the transducer gain of the circulator coupled paramp can be expressed as:

$$G_T = \left| \frac{- G_o + N^2 \left[G_1 + Y_{11} - \dfrac{\omega_1 \omega_2 \dfrac{\Delta c^2}{2}}{D^2 \left[Y_2 + Y_{22} \right]} \right]}{+ G_o + N^2 \left[G_1 + Y_{11} - \dfrac{\omega_1 \omega_2 \dfrac{\Delta c^2}{2}}{D^2 \left[Y_2 + Y_{22} \right]} \right]} \right| \qquad (3\text{-}13)$$

APPENDIX IV

MEASUREMENTS MADE ON VARIOUS TYPES OF VARACTORS

Diode # WE 1 — Line Z 17

Frequency (MC)	2100	2200	2300	2400	2500	2600	2700	2800	2900
Volts (DC)	.32	.41	.37	.3	.25	.2	.17	.13	.15

WE 2 — 17

Frequency	2100	2200	2300	2400	2500	2600	2700	2800	2900
Volts	.35	.42	.35	.27	.23	.23	.15	.15	.15

WE 3 — 17

Frequency	2100	2200	2300	2400	2500	2600	2700	2800	2900
Volts	.33	.38	.45	.32	.31	.25	.23	.2	.2

WE 4 — 17

Frequency	2100	2200	2300	2400	2500	2600	2700	2800	2900
Volts	.35	.45	.46	.37	.38	.35	.25	.22	.2

203 — 17

Frequency	1800	1900	2000	2100	2200	2300	2400	2500	2600
Volts	0	.1	.22	.1	.075	.45	.18	.06	.19

204 — 17

Frequency	1800	1900	2000	2100	2200	2300	2400	2500	2600
Volts	.03	.06	.075	.125	.1	.07	.025	0	.02

202 — 17

Frequency	1800	1900	2000	2100	2200	2300	2400	2500	2600
Volts	.03	.05	.05	.05	.09	.075	.025	.01	.01

205 — 17

Frequency	1800	1900	2000	2100	2200	2300	2400	2500	2600
Volts	.03	.03	.06	.19	.04	.1	0	.01	.02

206 — 17

Frequency	1800	1900	2000	2100	2200	2300	2400	2500	2600
Volts	.01	.03	.05	.22	.07	.15	.1	.03	.05

207 — 17

Frequency	1800	1900	2000	2100	2200	2300	2400	2500	2600
Volts	.02	.03	.09	.05	.03	.13	.04	.04	.06

208 — 17

Frequency	1800	1900	2000	2100	2200	2300	2400	2500	2600
Volts	.02	.04	.015	.12	.125	.13	.15	.14	.07

9A — 17

Frequency	1800	1900	2000	2100	2200	2300	2400	2500	2600
Volts	.075	.1	.175	.18	.195	.17	.12	.075	.08

10A — 17

Frequency	2200	2300	2400	2500	2600	2700	2800	2900	3000
Volts	.05	.075	.05	.075	.12	.25	.27	.05	.11

11A — 17

Frequency	2700	2800	2900	3000	3100	3200	3300	3400	3500
Volts	.07	.23	.3	.21	.2	.33	.36	.12	.3

2 — 17

Frequency	2100	2200	2300	2400	2500	2600	2700	2800	2900
Volts	0	.01	.02	.025	.02	.04	.075	.14	.2

Diode #	Line Z		2100	2200	2300	2400	2500	2600	2700	2800	2900
3	17	Frequency (MC) Volts (DC)	.01	.025	.06	.09	.07	.075	.095	.075	.05
5	17	Frequency Volts	.14	.25	.34	.25	.16	.22	.11	.05	.06
7	17	Frequency Volts	.12	.25	.33	.23	.18	.1	.05	.07	.07
9	17	Frequency Volts	.16	.24	.22	.125	.07	.1	.025	.02	.01
11	17	Frequency Volts	.04	.08	.16	.125	.075	.12	.1	.05	.025
12	17	Frequency Volts	.08	0	0	0	0	0	0	0	0
13	17	Frequency Volts	.05	.13	.05	0	0	0	0	0	0
14	17	Frequency Volts	0	0	0	.01	.025	.075	.175	.025	0
15	17	Frequency Volts	.25	.275	.2	.13	.1	.05	.05	.06	.06
16	17	Frequency Volts	.15	.1	.06	.02	.02	.02	0	0	0
18	17	Frequency Volts	.1	.14	.025	.02	0	0	0	0	0
20	17	Frequency Volts	.05	.09	.05	.03	.02	.02	.02	0	0
21	17	Frequency Volts	.09	.15	.25	.15	.125	.125	.12	.075	.025
22	17	Frequency Volts	.2	.26	.2	.12	.09	.09	.075	.05	.04
23	17	Frequency Volts	.03	.042	.032	.025	.02	.02	.01	0	0
27	17	Frequency Volts	.05	.05	.05	.045	.045	.045	.04	.035	.03

Diode #	Line Z	Frequency (MC)	2100	2200	2300	2400	2500	2600	2700	2800	2900
31	17	Volts (DC)	.03	.015	0	0	0	0	0	0	0

Diode #	Line Z		2100	2200	2300	2400	2500	2600	2700	2800	2900
32	17	Frequency	2100	2200	2300	2400	2500	2600	2700	2800	2900
		Volts	.175	.05	.025	0	0	0	0	0	0

30   NO RESPONSE

209	17	Frequency	1800	1900	2000	2100	2200	2300	2400	2500	2600
		Volts	.05	.15	.17	.14	.175	.19	.14	.03	.025

210	17	Frequency	1800	1900	2000	2100	2200	2300	2400	2500	2600
		Volts	.025	.07	.1	.1	.12	.15	.17	.07	.025

211	17	Frequency	1800	1900	2000	2100	2200	2300	2400	2500	2600
		Volts	.1	.125	.13	.11	.125	.1	.07	.03	.025

212	17	Frequency	1800	1900	2000	2 100	2200	2300	2400	2500	2600
		Volts	.03	.05	.07	.1	.12	.175	.185	.07	.01

213	17	Frequency	1800	1900	2000	2100	2200	2300	2400	2500	2600
		Volts	.07	.1	.075	.075	.11	.12	.07	.01	.02

214	17	Frequency	1800	1900	2000	2100	2200	2300	2400	2500	2600
		Volts	.01	.025	.04	.05	.075	.125	.15	.09	.025

215	17	Frequency	2300	2400	2500	2600	2700	2800	2900	3000	3100
		Volts	.2	.35	.36	.2	.15	.2	.22	.12	.17

216	17	Frequency	1800	1900	2000	2100	2200	2300	2400	2500	2600
		Volts	.07	.1	.22	.27	.22	.18	.13	.07	.02

217	17	Frequency	1800	1900	2000	2100	2200	2300	2400	2500	2600
		Volts	.11	.12	.07	.08	.25	.32	.17	.07	.1

218	17	Frequency	2100	2200	2300	2400	2500	2600	2700	2800	2900
		Volts	.25	.27	.14	.1	.1	.1	.12	.07	.07

219	17	Frequency	1800	1900	2000	2100	2200	2300	2400	2500	2600
		Volts	.2	.3	.3	.3	.25	.04	.02	.02	.02

220	17	Frequency	2000	2100	2200	2300	2400	2500	2600	2700	2800
		Volts	.25	.22	.2	.3	.4	.23	.12	.1	.14

/A 9A	7	Frequency	1800	1900	2000	2100	2200	2300	2400	2500	2600
		Volts	.13	.2	.24	.27	.3	.2	.07	.01	0

Diode #	Line Z	Frequency (MC)								
/A 10A	7	Volts (DC)	2300 / .07	2400 / .14	2500 / .25	2600 / .2	2700 / .4	2800 / .42	2900 / .2	3000 / .1

/A 11A	7	Frequency	2700	2800	2900	3000	3100	3200	3300	3400
		Volts	.1	.15	.22	.4	.52	.5	.53	.05

2	7	Frequency	2000	2100	2200	2300	2400	2500	2600	2700	2800
		Volts	0	0	0	0	0	0	.01	.015	.03

3	7	Frequency	2000	2100	2200	2300	2400	2500	2600	2700	2800
		Volts	0	.02	.025	.07	.1	.1	.1	.075	.025

5	7	Frequency	2000	2100	2200	2300	2400	2500	2600	2700	2800
		Volts	0	0	0	.03	.07	.1	.15	.17	.1

7	7	Frequency	2000	2100	2200	2300	2400	2500	2600	2700	2800
		Volts	.10	.15	.20	.27	.40	.40	.25	.05	0

9	7	Frequency	2000	2100	2200	2300	2400	2500	2600	2700	2800
		Volts	.15	.2	.4	.15	.05	0	0	0	0

11	7	Frequency	2100	2200	2300	2400	2500	2600	2700	2800	2900
		Volts	.05	.1	.19	.27	.2	.12	.06	0	0

13	7	Frequency	2100	2200	2300	2400	2500	2600	2700	2800	2900
		Volts	.075	.14	.03	0	0	0	0	0	0

12	7	Frequency	1900	2000	2100	2200
		Volts	.02	.01	0	0

14	7	Frequency	2100	2200	2300	2400	2500	2600	2700	2800	2900
		Volts	0	0	0	.02	.05	.075	.175	.3	.1

15	7	Frequency	2100	2200	2300	2400	2500	2600	2700	2800	2900
		Volts	.3	.4	.12	.05	.02	0	0	0	0

16	7	Frequency	1900	2000	2100	2200	2300	2400	2500	2600	2700
		Volts	.1	.15	.14	.1	.05	.04	.02	0	0

18	7	Frequency	2000	2100	2200	2300	2400	2500	2600	2700	2800
		Volts	.17	.14	.1	.025	0	0	0	0	0

20	7	Frequency	2000	2100	2200	2300	2400	2500	2600	2700	2800
		Volts	.05	.07	.09	.08	.06	.04	.03	.025	.02

21	7	Frequency	2000	2100	2200	2300	2400	2500	2600	2700	2800
		Volts	.1	.1	.15	.2	.26	.31	.22	.22	.15

Diode #	Line Z	Frequency (MC)	2000	2100	2200	2300	2400	2500	2600	2700	2800
22	7	Volts (DC)	.15	.2	.25	.33	.2	.13	.1	.07	.05

26	7	Frequency	2000	2100	2200	2300	2400	2500	2600	2700	2800
		Volts	.05	.07	.082	.07	.06	.03	.025	.02	.01

27	7	Frequency	2000	2100	2200	2300	2400	2500	2600	2700	2800
		Volts	.005	.004	.003	.005	.002	.002	.001	.002	.001

30   NO RESPONSE

31	7	Frequency	2000	2100	2200	2300
		Volts	.02	.015	.01	0

32	7	Frequency	1800	1900	2000	2100	2200	2300
		Volts	.2	.24	.15	.09	0	0

WE 1	7	Frequency	1800	1900	2000	2100	2200	2300	2400	2500	2600
		Volts	.31	.31	.34	.37	.4	.35	.25	.2	.2

WE 2	7	Frequency	1800	1900	2000	2100	2200	2300	2400	2500	2600
		Volts	.32	.33	.37	.38	.3	.2	.13	.12	.1

WE 3	7	Frequency	2000	2100	2200	2300	2400	2500	2600	2700	2800
		Volts	.33	.37	.4	.3	.25	.17	.17	.15	.1

WE 4	7	Frequency	2000	2100	2200	2300	2400	2500	2600	2700	2800
		Volts	.35	.4	.45	.35	.25	.2	.2	.15	.07

/A 202	7	Frequency	1800	1900	2000	2100	2200	2300	2400	2500	2600
		Volts	.15	.25	.37	.35	.42	.2	.07	.01	0

/A 203	7	Frequency	1800	1900	2000	2100	2200	2300	2400	2500	2600
		Volts	.08	.08	.2	.22	.18	.35	.5	.32	.1

/A 204	7	Frequency	1800	1900	2000	2100	2200	2300	2400	2500	2600
		Volts	.07	.1	.24	.23	.17	.34	.4	.2	.05

/A 205	7	Frequency	1800	1900	2000	2100	2200	2300	2400	2500	2600
		Volts	.16	.24	.35	.25	.3	.2	.03	0	0

/A 206	7	Frequency	1800	1900	2000	2100	2200	2300	2400	2500	2600
		Volts	.24	.3	.45	.35	.37	.15	.05	.02	0

/A 207	7	Frequency	1800	1900	2000	2100	2200	2300	2400	2500	2600
		Volts	.06	.05	.14	.12	.08	.1	.19	.21	.2

Diode #	Line Z	Frequency (MC)	1800	1900	2000	2100	2200	2300	2400	2500	2600
/A 208	7	Volts (DC)	.1	.12	.26	.22	.26	.38	.31	.2	.1

/A 209	7	Frequency	1800	1900	2000	2100	2200	2300	2400	2500	2600
		Volts	.15	.2	.34	.27	.37	.45	.3	.15	.05

/A 210	7	Frequency	1800	1900	2000	2100	2200	2300	2400	2500	2600
		Volts	.1	.1	.25	.27	.23	.3	.35	.23	.15

/A 211	7	Frequency	1800	1900	2000	2100	2200	2300	2400	2500	2600
		Volts	.1	.15	.3	.2	.25	.15	.07	.03	.01

/A 212	7	Frequency	1800	1900	2000	2100	2200	2300	2400	2500	2600
		Volts	.07	.08	.2	.25	.2	.28	.32	.3	.2

/A 213	7	Frequency	1800	1900	2000	2100	2200	2300	2400	2500	2600
		Volts	.3	.4	.35	.22	.22	.1	.01	0	0

/A 214	7	Frequency	1800	1900	2000	2100	2200	2300	2400	2500	2600
		Volts	.06	.06	.2	.17	.15	.25	.27	.2	.15

/A 215	7	Frequency	2000	2100	2200	2300	2400	2500	2600	2700	2800
		Volts	.16	.25	.26	.5	.63	.65	.55	.3	.2

/A 216	7	Frequency	1800	1900	2000	2100	2200	2300	2400	2500	2600
		Volts	.17	.24	.35	.28	.33	.15	.05	0	0

/A 217	7	Frequency	1800	1900	2000	2100	2200	2300	2400	2500	2600
		Volts	0	.1	.3	.35	.37	.45	.3	.08	.05

/A 218	7	Frequency	1800	1900	2000	2100	2200	2300	2400	2500	2600
		Volts	0	0	.05	.1	.1	.15	.2	.35	.25

/A 219	7	Frequency	1800	1900	2000	2100	2200	2300	2400	2500	2600
		Volts	.18	.25	.4	.32	.2	.05	.01	0	0

/A 220	7	Frequency	1800	1900	2000	2100	2200	2300	2400	2500	2600
		Volts	0	.1	.23	.27	.3	.47	.4	.25	.1

/A 9A Ku Band Mount	7	Frequency	2100	2200	2300	2400	2500	2600	2700	2800	2900
		Volts	0	.2	.45	.2	.15	.15	.05	.02	0

/A 11A Ku Band Mount	7	Frequency	2800	2900	3000	3100	3200	3300	3400	3500	3600
		Volts	.2	.4	.6	.63	.7	.5	.3	.23	.2

Diode #	Line Z	Frequency	(MC)	2100	2200	2300	2400	2500	2600	2700	2800
/A 9A Ku Band Mount	20	Volts	(DC)	0	.01	.05	.18	.13	.23	.1	.05
/A 202 Ku Band Mount	17	Frequency Volts		2100 0	2200 0	2300 .01	2400 .02	2500 .03	2600 .02	2700 .01	2800 0

APPENDIX V

PERFORMANCE DATA ON FERRITE CIRCULATORS

A. Manufacturers Data   (Melabs)

Melabs Model X-343, Serial #1

Frequency (Kmc)	VSWR	Insertion Loss Arms 1-2 (db)	Isolation Arms 1-3 (db)
3.0	1.16	.20	23.0
3.2	1.11	.10	28.0
3.5	1.07	.05	28.0
3.8	1.08	.10	30.0
4.0	1.17	.20	21.5

Melabs Model X-344, Serial #1

Frequency (Kmc)	VSWR	Insertion Loss Arms 1-2 (db)	Isolation Arms 1-3 (db)
2.0	1.22	.20	18.5
2.2	1.15	.15	25.0
2.5	1.03	.10	28.5
2.8	1.14	.10	31.0
3.0	1.25	.15	20.7

B. Measured Data

Melabs Model X-343, Serial #1

Frequency (Kmc)	VSWR	Isolation Arms 1-3 (db)
3.0	1.06	20.5
3.2	1.16	22.7
3.4	1.10	24.0
3.6	1.16	27.2
3.8	1.21	36.5
4.0	1.21	29.5

AD ___
Accession Number ___

Surface Communications Systems Laboratory
Radio Corporation of America, New York 13, New York

BROADBAND S-BAND REACTANCE AMPLIFIER
by B. Bossard, R. M. Kurzrok,
E. Markard, B. Perlman
and R. Petkal

Rept. for 1 July 1960 - 7 March 1962 on DA Project No. 3A99-21-001-01
101 p. incl. illustrations
(Scientific Report No. 6 - Final Report)
Contract DA-36-039-sc-85058 Unclassified Report

A substantial amount of small-signal and large-signal theoretical work has been carried out for the broadbanding of microwave parametric amplifiers. Theoretical results have yielded single-diode voltage-gain-bandwidth products of 3500 mc at "S" band. It is concluded that the simulation of broadband paramps by appropriate lumped-circuit elements is handicapped at microwave frequencies where inductances and capacitances must be simulated by distributed elements. Moreover, the sections of transmission line coupling the individual network elements to the varactor diode have frequency sensitivities of their own which must be considered in transforming a lumped-element design into a distributed microwave equivalent, especially when broad (20 - 50%) bandwidths are involved.

Broadband paramps can be constructed, however, by making maximum use of the varactor parasitic elements in a filter structure at the plane of the diode. (No coupling lengths of line are required.) Techniques have been developed which allow the varactor diode to exhibit two simultaneous resonant frequencies (at signal and idler) depending upon the geometry of the holding structure. Novel experimental techniques were conceived on the subject program that permit rapid determination of the diode resonances and matching conditions. The gain-bandwidth product of a given diode can be evaluated by distributed network efforts on parametric amplifiers employing the above principle have yielded single-diode voltage-gain-bandwidth products of 3300 mc at "S" band.

Unclassified

1. Amplifiers-Development
2. Diodes-Application
3. Semiconductors
4. Upconverters
   Circulator-Coupled Single-Diode Paramp
   Balanced Coaxial Paramp
I. Title: Parametric Amplifiers
II. Bossard, B., Kurzrok, R.M., Markard, E., Perlman, B., and Petkal, R.
III. Army Signal Research and Development Laboratory, Ft. Monmouth, N.J.
IV. Contract DA-36-039-sc-85058

Armed Service Technical Information Agency

DA36-039 sc-85058   Final Report
Radio Corporation of America   1 July 60 - 7 March 62

<u>Distribution List</u>

                                                       <u># of Copies</u>

OASD (R&E), Rm1065
The Pentagon
Attn: Technical Library
Washington 25, D. C.   1

Chief of Research & Development
OCS, Department of the Army
Washington 25, D. C.   1

Commanding General
U. S. Army Electronics Command
Attn: AMSEL-CG
Fort Monmouth, New Jersey   1

Director
U. S. Naval Research Laboratory
Attn: Code 2027
Washington 25, D. C.   1

Commanding Officer and Director
U. S. Navy Electronics Laboratory
San Diego 52, California   1

Commander
Wright Air Development Center
Attn: WCOSI-3
Wright-Patterson Air Force Base, Ohio   2

Commander
Air Force Cambridge Research Laboratories
Attn: Research Library CRXL-R
L. G. Hanscom Field
Bedford, Massachusetts   1

Commander
Rome Air Development Center
Attn: RAALD
Griffiss Air Force Base, New York   1

Commander
Armed Services Technical Information Agency
Arlington Hall Station
Arlington 12, Virginia   10

DA36-039 sc-85058	# of Copies

Chief
U. S. Army Security Agency
Arlington Hall Station
Arlington 12, Virginia — 2

Deputy President
U. S. Army Security Agency Board
Arlington Hall Station
Arlington 12, Virginia — 1

Commanding Officer
Diamond Ordnance Fuze Laboratories
Attn: Library, Rm. 211, Bldg. 92
Washington 25, D. C. — 1

Commanding Officer
U. S. Army Electronics Materiel Support Agency
Attn: SELMS-ADJ
Fort Monmouth, New Jersey — 1

Corps of Engineers Liaison Office
U. S. Army Electronics R&D Laboratory
Fort Monmouth, New Jersey — 1

Marine Corps Liaison Office
U. S. Army Electronics R&D Laboratory
Fort Monmouth, New Jersey — 1

Advisory Group on Electron Devices
346 Broadway
New York 13, New York — 2

Hughes Research Laboratories
Attn: Ralph Weglein
Malibu, California — 1

Sylvania Electric Products
100 Sylvan Road
Attn: E. Feldman
Woburn, Massachusetts — 1

Philco Corporation
Attn: Nels Hoffman
Special Products Division
Lansdale, Pennsylvania — 1

DA36-039 sc-85058

Microwave Associates, Inc.
Northwest Industrial Park
Attn: Howard Ellowitz
Burlington, Massachusetts   1

Naval Material Laboratory
Attn: Paul Giordano, Code 924
New York Naval Shipyard
Brooklyn 1, New York   1

Micromega Corp.
4134 Del Ray Avenue
Attn: Dr. Bu
Venice, California   1

SFD Labs
Attn: H. T. Closson
Union, New Jersey   1

Bell Telephone Laboratories
Attn: R. M. Ryder
Murray Hill, New Jersey   1

Bell Telephone Laboratories
Attn: Harry Elder
555 Union Blvd.
Allentown, Pennsylvania   1

Department of the Navy
Bureau of Ships
Attn: A. H. Young
Semiconductor Unit, Code 691A
Washington 25, D. C.   1

Airborne Instruments Laboratory
A Division of Cutler-Hammer, Inc.
Attn: Mr. Pete Lombardo
Deer Park, Long Island, New York   1

Texas Instruments, Inc.
P. O. Box 5012
Dallas 22, Texas   1

TRG
Attn: Mr. J. Kliphuis
Syosset, Long Island, New York   1

DA36-039 sc-85058   # of Copies

Mr. A. Mayer
Sylvania EDL
P. O. Box 205
Mt. View, California   1

Commanding Officer
U. S. Army Electronic Materiel Agency
Attn: SELMA-R2b
Industrial Preparedness Activity
225 South 18th Street
Philadelphia 3, Pennsylvania   1

Commanding Officer
U. S. Army Electronics R&D Laboratory
Fort Monmouth, New Jersey
Attn: Director of Research   1
Attn: Technical Documents Center   1
Attn: Technical Information Division   3
Attn: Ch, S&M Br., Solid State & Freq Cont Division   1
Attn: Rpts Dist Unit, Solid State & Freq Cont Div (Record cy)   1
Attn: Herbert Brett, Countermeasures Div, Surveillance Dept   1
Attn: W. G. Matthei, Solid State & Frequency Control Division   1
Attn: F. Senko, M&QE Br., Solid State & Freq Cont Division   7

Total number of copies to be distributed   60

Watkins-Johnson Company
3333 Hillview Avenue
Attn: H. Richard Johnson
Stanford Industrial Park
Palo Alto, California   1

This contract is supervised by the Solid State & Frequency Control Division,
Electronic Components Department, USAELRDL, Fort Monmouth, New Jersey. For
further technical information contact Mr. F. P. Senko, Project Engineer.
Telephone 53-52352.

GENERAL DISTRIBUTION LIST

Vice President, Research
RCA Laboratories
Princeton, N.J.

Patent Department
Princeton, N.J.

Library
Surface Communications Systems Laboratories
New York City

Library
DEP Central Engineering
Camden, New Jersey

Engineering Publications
Surface Communications Systems Laboratories (4 Copies)
New York City

Library
Surface Communications Systems Laboratories
Tucson, Arizona

SPECIAL DISTRIBUTION LIST

Bradburd, E.M.	RCA, New York
Cochran, S.W.	RCA, Camden
Cunningham, O.B.	RCA, Camden
Grassheim, I.	RCA, Camden
DeCredico, R.	RCA, Camden
Guenther, R.	RCA, New York
Guttmann, I.	RCA, New York
Holshouser, J.R.	RCA, New York
Kurzrok, R.M.	RCA, New York
Mack, A.	RCA, New York
Trevor, B.A.	RCA, Tucson
Twinam, J.R.	RCA, Tucson